A New Approach to Model a System with Both Friction and Geometric Nonlinearity

Drithi Shetty[1], **Kyusic Park**[1] **and Matthew S. Allen**[2]

[1]Graduate Student; University of Wisconsin-Madison - Department of Mechanical Engineering; email: ddshetty@wisc.edu, kpark93@wis
[2]Professor; Brigham Young University - Department of Mechanical Engineering; email: matt.allen@byu.edu

Abstract

This paper presents a new reduced-order model that can capture the nonlinear dynamics of a structure containing both friction and geometric nonlinearity, and proposes a procedure to derive the parameters of the model from quasi-static simulations. The Single-mode Implicit Condensation and Expansion (SICE) method was recently show to be capable of capturing the resonant behavior of a geometrically nonlinear structure, and the modal Iwan model has proven effective at capturing the hysteretic behavior of a mode that exhibits nonlinearity due to friction. This paper combines the two into a new model, referred to here as the Iwan model with Geometric Nonlinearity (or the IGNL model). It consists of an Iwan model with an additional spring-slider unit, where the slider has infinite strength and the spring consists of polynomial terms that define the SICE-ROM. A procedure is also proposed to use Quasi-Static Modal Analysis (QSMA) to estimate the parameters of the IGNL model from a set of nonlinear force-displacement curves. Existing literature shows how QSMA can be used to characterize the force-displacement behavior of a nonlinear mode where the nonlinearity is due to friction or bending-stretching coupling, but not both simultaneously. This paper proposes certain adjustments to the QSMA procedure so that the two forms of nonlinearity can be isolated. Two case studies are presented to test the efficacy of the IGNL model, one consisting of a simple spring-mass model and the second, a finite element model containing both contact and geometric nonlinearity. The proposed method is shown to be significantly faster than performing dynamic simulations to estimate the amplitude-dependent frequency and damping behavior.

Keywords: nonlinear dynamics, Masing model, hysteresis, quasi-static, reduced-order model

1 Introduction

The aircraft, spacecraft and automotive industries are increasingly making use of thin, curved panels in their structures for higher strength-to-weight ratios and lower fuel consumption. Such structures can exhibit geometric nonlinearities, caused by bending-stretching coupling under large deformations of the panels [1, 2]. As a result, the structure experiences significant changes in stiffness at high load amplitudes, and the dynamic behavior cannot be captured by linear vibration theory. Additionally, these structures often contain mechanical fasteners that are used to assemble the various parts, making manufacturing and future maintenance convenient. The use of fasteners, however, results in changes in stiffness as well as significant damping due to frictional energy losses at the interfaces [3, 4]. The contact pressure at the interface is not uniform, with higher pressure closer to the bolted joint and lower pressure further away [5]. Therefore, at lower amplitudes, the edges of the jointed surfaces slip while the region closer to the bolt hole remains mostly stuck. This is called microslip. In the microslip regime, the stiffness of the joint decreases slightly, whereas the damping has been observed to increase significantly [6–8], sometimes by orders of magnitude [9]. The response of a structure at resonance, and, as a result, to random excitation, depends on the damping [10]. Thus, it is important to estimate the damping due to friction at the interfaces.

Simulating the dynamic response of a geometrically nonlinear structure using a high-fidelity Finite Element (FE) model is highly computationally expensive. Therefore, several reduced-order models have been developed as an alternative. A reduced-order model for geometric nonlinearity will typically contain linear mass and stiffness terms along with additional higher-order polynomial stiffness terms, usually limited to quadratic and cubic terms. The polynomial coefficients can be estimated using static nonlinear solutions, as described in [11]. The methods that use static solutions can be classified as indirect, or non-intrusive evaluation methods, since they do not require manipulation of the nonlinear stiffness matrices in the FE package [12, 13]. Murayov and Rizzi [14] developed one such method, known as the Enforced Displacement (ED) procedure, where the nonlinear FE model is constrained to take the shape of the linear mode of interest, and the reaction forces needed to do so are calculated by a static analysis. This is done over a range of displacement amplitudes, with the resultant force-displacement

backbone curve being used to estimate the polynomial coefficients. In this method, both bending and stretching (i.e. axial or dual [12]) modes need to be included when defining the modal basis in order to capture the bending-stretching coupling.

Alternatively, McEwan et al. [15] presented the Implicit Condensation (IC) method where a static force is applied in the shape of the mode of interest and the resulting displacement field is estimated using the nonlinear FE model. This data is then used to estimate the nonlinear coefficients in the reduced model, similar to what is done in the ED method. In the IC method, however, the bending-stretching coupling is implicitly captured by applying a force instead of displacement. Thus, the axial modes do not need to be included in the basis. Hollkamp and Gordon [16] presented the Implicit Condensation and Expansion (ICE) method to recover the axial displacements or the corresponding stresses from the IC method. In both the ED and ICE methods, multiple modes can be considered simultaneously to account for modal coupling. Park and Allen [17] presented a single degree-of freedom ICE method, dubbed the SICE-ROM, where the nonlinear restoring force is approximated by a single, dominant mode. This ROM requires polynomial terms higher than just the third order, presumably to capture quasi-static coupling between the mode under consideration and all other modes. Park and Allen showed, for a few strongly nonlinear structures, that the dynamics near a single mode could be represented by a SICE-ROM with minimal loss of accuracy.

In case of friction nonlinearity, dynamic analysis of a finely meshed FE model with a friction element between every pair of nodes in contact is highly computationally expensive. Alternatively, each side of a contact interface can be treated as rigid with all its nodes tied to a single representative node. The appropriate ROM can then be applied between the representative nodes of the surfaces in contact, as done by [18] and others. Frictional systems are hysteretic in nature, meaning the response of the system is dependent on its current as well as past states. Hence, the ROM for a system with stick-slip friction must include hysteretic effects; the polynomial-based ROMs that work well for geometrically nonlinear systems do not capture hysteresis. Gaul and Nitsche [19] reviewed different hysteretic models that can be used to capture the dynamics due to bolted joints. More recently, Mathis et al. [20] presented an extensive review of various damping models and discussed the relation between them. Some of the models used for friction nonlinearity were originally developed to represent metal elastoplasticity [21–23]. One of the most commonly used hysteretic models is the Distributed-Element Model [23], also commonly referred to as the Iwan model. This model consists of an arrangement of linear spring and slider units, known as Jenkins elements. The sliders have varying strengths, resulting in a specific nonlinear force-displacement relationship. Since it is composed of Jenkins elements, the Iwan model falls under the category of Masing models [24, 25]. This implies that the force-displacement curve of the Iwan model is symmetric about the origin and the complete hysteresis loop at any amplitude can be estimated, using Masing's rules [25], from the backbone curve calculated up to that amplitude.

The approach above produces a reduced model in which the physics and geometry of the structure are preserved and each joint exists physically at some location within the model. However, few, if any, methods exist that allow one to compute the parameters of the hysteretic model from first principles. Instead, tests are typically performed on the structure and then the parameters of the hysteretic model are adjusted until agreement is obtained. While this is attractive in many applications, if a structure has multiple joints then each can contribute to the overall system dynamics, and this coupling between the joints makes it challenging to estimate the parameters of each hysteretic model. To circumvent this problem, Segalman [26] proposed a modal approach in which each nonlinear mode can be represented by a single degree-of-freedom (SDOF) system, with the corresponding nonlinear restoring force given by a constitutive hysteretic model. In essence, this approach is similar to using a SICE or one-mode ICE ROM to obtain a reduced model that captures the dynamics of the nonlinear mode of the system. Such a model is far easier to identify from experimental measurements, or using quasi-static analysis as done by Lacayo and Allen [27]. While Segalman's approach works well to estimate the dynamics of a mode of interest, there is currently not a standard way of creating a multi-mode hysteretic model for a system with frictional nonlinearity, so this issue is not addressed in this work. This work focuses on one degree-of-freedom, modal reduced-order models.

Just as a SICE-ROM, for a geometrically nonlinear system, can be estimated from force-displacement data, a hysteretic nonlinear modal model for a system with frictional nonlinearity can also be estimated from force-displacement data from a detailed finite element model. A few different quasi-static methods have been developed for doing so. Festjens et al. [28] presented a method in which a quasi-static distributed load was applied such that it represented the inertial loading when the structure vibrates in the mode of interest. The corresponding displacement can then be calculated using any finite element package. This was done over a range of load amplitudes to obtain the force-displacement curve. While Festjens et al. adjusted the loading as the mode shape of the structure changed, Lacayo and Allen [27] proposed a simplification where they used a loading with a constant shape to excite the mode in question. As the joint slips the actual deflection of the structure, or the effective mode shape, does change, but the loading is not updated to account for this. Their method is called the method of Quasi-Static Modal Analysis, or QSMA. Its efficacy has been tested on various systems consisting of friction nonlinearity [29–31]. Balaji and Brake [32] proposed a variation of QSMA, known as Rayleigh-Quotient based Nonlinear Modal Analysis (RQNMA), where they extended the concept of Rayleigh quotients to both conservative and non-conservative nonlinear systems. Their method updates the applied static load as the mode shapes change and hence was shown to be more accurate than QSMA for a system

where the modes become highly localized as the vibration level increases.

The existing reduced-order modeling approaches discussed so far consider either geometric or friction nonlinearity. For a structure exhibiting both forms of nonlinearity, one could use the ICE methods, thus ignoring the effect of friction, or use hysteretic models and ignore the effect of geometric nonlinearity. Both these approaches lead to a loss of accuracy. Alternatively, one could simulate the transient dynamic response of the full structure using a high-fidelity FE model. However, this is exceedingly computationally expensive. Kuether et al. [33] found that a cluster of 9 nodes and 432 cores, with 192 GB RAM per node, was required to simulate 0.25 s of dynamic response of a high-fidelity 3D FE model of a structure with friction and geometric nonlinearity in 48 hours. This paper presents a reduced-order modeling technique for characterizing a nonlinear mode of a structure by combining the SICE-ROM with the modal Iwan Model to represent the nonlinearity arising from both friction and bending-stretching coupling. The resulting ROM is referred to as an Iwan model with Geometric Nonlinearity, or an IGNL model. The paper also presents an approach to identify the parameters of the IGNL model using QSMA. It shows how the effects of the two types of nonlinearity on the force-displacement behavior can be isolated, assuming the interactions between them are weak enough for superposition to hold. Two case studies are presented to evaluate the ability of the IGNL model to capture the amplitude-dependent frequency and damping behavior of a nonlinear mode of interest. The paper also shows that the proposed method is significantly faster than performing a dynamic simulation, and is more accurate than fitting just a SICE-ROM or a hysteretic model.

The next section provides theoretical background for QSMA, the SICE-ROM and the Iwan Model. In Sec. 3, the proposed IGNL model is formulated and the method to estimate the frequency and damping from this model is presented. Section 4 presents a simple numerical case study where the proposed approach is applied to a single-degree-of-freedom system with a cubic spring and an Iwan element. This is followed, in Sec. 5, by a more complex case study using a two-dimensional finite element model of the Tribomechadynamics Benchmark Structure [34], which is composed of a curved panel that is clamped at the ends using bolts. Finally, the conclusions are presented in Sec. 6.

2 Background

2.1 Overview of Quasi-Static Modal Analysis

Lacayo and Allen [27] showed that the method of Quasi-Static Modal Analysis (QSMA) can be used to calculate the force-displacement relation for a nonlinear mode of a jointed structure consisting only of friction nonlinearity. Park and Allen [17] derived a similar relation for a single mode of a geometrically nonlinear structure. Both of these methods are reviewed here. Consider a Finite Element (FE) model of a structure, the Equations of Motion (EoM) for which can be written as

$$\mathbf{M}\ddot{\mathbf{x}} + \mathbf{C}\dot{\mathbf{x}} + \mathbf{K}\mathbf{x} + \mathbf{f}_{\mathrm{nl}}(\mathbf{x}, \boldsymbol{\theta}) = \mathbf{f}_{\mathrm{ext}} \tag{1}$$

where $\mathbf{M}, \mathbf{C}, \mathbf{K}$ are the mass, damping and stiffness matrices, respectively, and $\mathbf{x}, \dot{\mathbf{x}}, \ddot{\mathbf{x}}$ are the displacement, velocity and acceleration vectors, respectively. The vector of nonlinear forces, $\mathbf{f}_{\mathrm{nl}}(\mathbf{x}, \boldsymbol{\theta})$, is a function of displacement and a vector of variables, $\boldsymbol{\theta}$, that depend on the past state of the system. The definition of $\boldsymbol{\theta}$ depends on the type of hysteretic model used. In the Iwan model, for example, it represents a vector that captures the state of the sliders that form the model. The equations can be linearized about some state of interest, to capture the behavior for small vibrations about that state. Without loss of generality, the equations above are assumed to be linearized about $\mathbf{x} = 0$ to estimate the low-amplitude modal frequencies, $\boldsymbol{\omega}_0$, and linear mode-shapes, $\boldsymbol{\Phi}$, by performing an eigen-value analysis. Then, a static load is applied such that it excites only the r^{th} mode of the system. The applied load must be $f_{\mathrm{ext}} = \mathbf{M}\boldsymbol{\Phi}_r$, where $\boldsymbol{\Phi}_r$ is the low-amplitude linear mode shape of the r^{th} mode of interest [27]. This results in the following quasi-static problem:

$$\mathbf{K}\mathbf{x} + \mathbf{f}_{\mathrm{nl}}(\mathbf{x}, \boldsymbol{\theta}) = \boldsymbol{\alpha}\mathbf{M}\boldsymbol{\Phi}_{\mathbf{r}}. \tag{2}$$

Equation 2 can be solved to obtain $\mathbf{x}$ for different force amplitude levels, $\boldsymbol{\alpha}$. Typically, the structure starts in equilibrium and $\boldsymbol{\alpha}$ is chosen to be monotonically increasing. This gives the initial loading behavior, also known as the backbone curve. To retrieve the force-displacement relation of the r^{th} mode, the force applied to the structure and the displacement calculated are converted from the physical to the modal domain, using Eqs. 3 and 4.

$$\mathbf{f}_{\mathrm{modal}} = \boldsymbol{\Phi}_r^{\mathrm{T}}\boldsymbol{\alpha}\mathbf{M}\boldsymbol{\Phi}_r = \boldsymbol{\alpha} \tag{3}$$

$$q_r(\alpha) = \boldsymbol{\Phi}_r^T\mathbf{M}x(\alpha) \tag{4}$$

In this way, the force-displacement relation for the nonlinear mode of a structure, $\boldsymbol{\alpha}$ versus $\mathbf{q}_r(\boldsymbol{\alpha})$, can be calculated by solving a quasi-static problem. However, further post-processing is required to estimate the amplitude-dependent frequency and damping for the mode under consideration, as discussed in the following sections.

2.2 SICE-ROM for Geometric Nonlinearity

Park and Allen [17] derived a Reduced Order Model (ROM) for strongly nonlinear structures using QSMA, that is briefly summarized here. The undamped SDOF EoM of the r^{th} mode is assumed to have the following form,

$$\ddot{q}_r + \omega_r^2 q_r + \theta_{\text{gnl}}(q_r) = \mathbf{\Phi}_r^{\text{T}} \mathbf{f}_{\text{ext}} \tag{5}$$

where $\theta_{\text{gnl}}(q_r)$ is the nonlinear restoring force approximated by the r^{th} mode only. This restoring force can be obtained from the quasi-static solution calculated using the method described in Sec. 2.1. Note here that this model form is not dependent on any hysteretic variable $\boldsymbol{\theta}$. Next, a polynomial can be used to approximate this restoring force function, as given by Eq. 6,

$$\theta_{\text{gnl}}(q_r) = \sum_{j=2}^{m} k_j q_r^j, \tag{6}$$

where k_j is the j^{th} nonlinear stiffness coefficient and m is the highest order of the polynomial. Higher order polynomials are required for modes that exhibit strong static coupling. The coefficients, k_j, can be estimated from the quasi-static force-displacement data by applying the method of least squares, as elaborated in [17]. This approach minimizes the cost function, J, given by Eq. 7,

$$\min_{k_j} J = \frac{1}{S} \sum_{l=1}^{S} \frac{\left(\omega_r^2 q_{r,l} + \sum_{j=2}^{m} k_j (q_{r,l})^j - \alpha_l\right)^2}{\alpha_l^2} \tag{7}$$

where S is the number of sample points in the QSMA analysis, i.e. the length of the vector $\boldsymbol{\alpha}$. The resulting ROM is called the single degree-of-freedom implicit condensation and expansion, or SICE-ROM. Once a ROM of this form is fit, the frequency behavior can be estimated using numerical continuation techniques, as discussed in Sec. 3.3. Park and Allen also showed three different case studies, where the SICE-ROM was used to successfully characterize the geometric nonlinearity of structures with varying complexity, thus verifying the method's capabilities. It must be noted that this ROM only accounts for static coupling between modes. In case of dynamic coupling, the single-mode quasi-static backbone curve cannot be used to accurately predict the dynamic response, even when higher-order polynomials are used. Additionally, since this is an SDOF ROM, it cannot capture any internal resonances in the Nonlinear Normal Mode (NNM). As discussed in [17], this can be an advantage in some applications, such as model updating. The method proposed in this work shares these limitations; it only estimates the behavior of a single, uncoupled mode.

2.3 Iwan Model for Friction Nonlinearity

In a built-up structure, hysteretic constitutive models are used to simulate the nonlinearity due to friction. The Distributed Element Model, developed by Iwan [23], is one such lumped, mathematical model. It consists of a series of elasto-plastic units, known as Jenkins elements, arranged as shown in Fig. 1a. The springs in all the elasto-plastic units are identical, while the sliders have varying yield levels. The restoring force calculations for such a model have been derived in [23], with a brief summary of the same included here.

By definition, each Jenkins element exhibits bi-linear behavior. During initial loading, an element may either lie in the region OA or AB of the plot shown in Fig. 1b, depending on its slip force. Thus, the force-displacement relation, in case of positive loading, for each element is given by Eq. 8,

$$\begin{aligned} f_i &= \frac{kx}{N}; \qquad \dot{x} > 0, 0 < kx/N \leq f_i^*/N \\ f_i &= \frac{f_i^*}{N}; \qquad \dot{x} > 0, kx/N > f_i^*/N \end{aligned} \tag{8}$$

where k/N is the stiffness of each element, f_i^*/N is the yield force of each element, and N is the total number of elements. To calculate the force-displacement relation for the whole model, the number of elements that have yielded (or slipped) and those that are still stuck need to be considered separately. If n out of N elements have yielded (i.e. they have $kx/N > f_i^*/N$), their contribution to the total force can be given as

$$\sum_{i=1}^{n} \frac{f_i^*}{N} \tag{9}$$

while those that have not yet yielded, (i.e. they have $kx/N \leq f_i^*/N$) can be written as

$$\frac{k}{N} x(N-n) \tag{10}$$

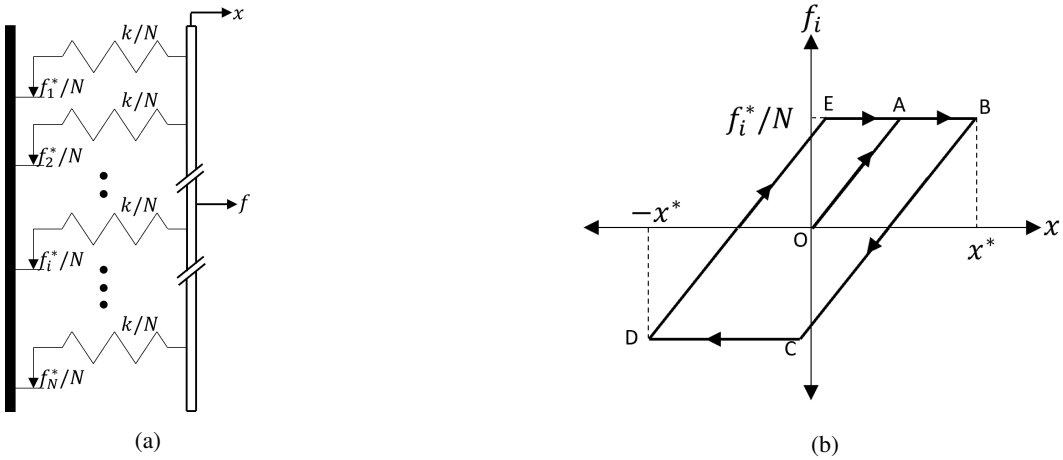

Figure 1: (a) Illustration of the Distributed Element (or Iwan) Model, and (b) The bi-linear force-displacement relationship of a Jenkins element

The total force during initial loading can, therefore, be written as shown in Eq. 11.

$$f = \sum_{i=1}^{n} \frac{f_i^*}{N} + \frac{k}{N} x(N-n); \qquad \dot{x} > 0 \tag{11}$$

If the direction of loading is reversed, i.e. $\dot{x} < 0$, all the elements will switch to a stuck state at the reversal point. As the reverse loading amplitude increases, the elements that did not yield during loading will remain unyielded. However, the elements that did yield during loading could have one of two states - either they will continue to be in a positive yield state or they will switch to a negative yield state. For an element that has already yielded in the positive direction to also yield in the negative direction, $k(x^* - x)$ must be greater than $2f_i^*$, where x^* is the displacement at which reversal occurs. Relationships similar to Eq. 8 can be written for the unloading case for each Jenkins element (see [23]). The total restoring force in the unloading direction is given by

$$f_{\text{rev}} = \sum_{i=1}^{n'} \frac{-f_i^*}{N} + \sum_{i=n'}^{n} \left[\frac{f_i^*}{N} - \frac{k}{N}(x^* - x) \right] + \frac{k}{N} x(N-n); \qquad \dot{x} < 0,\ -x^* \leq x \leq x^* \tag{12}$$

where n' is the number of elements that have yielded in the negative direction. Note that the first term on the right-hand side of Eq. 12 corresponds to the Jenkins elements that lie in the region CD of Fig. 1b, the second term corresponds to those that lie in the region BC and the final term corresponds to those that remain stuck and retrace their path along OA. For an infinite distribution of elements (i.e. N becomes very large), Eqs. 11 and 12 can be written in integral form instead of summations; this can be found in [23]. Note that in the integral form, a distribution function is defined that specifies the fraction of the total elements that yields at every force value. The Iwan model can take different forms, based on the distribution function specified. For example, the four-parameter Iwan model [35] implements a power-law distribution function and is commonly used to model friction nonlinearity due to bolted joints (and will be used in the case study presented in Sec. 4).

3 Proposed Approach

3.1 Iwan Model with Geometric Nonlinearity (IGNL model)

This paper proposes a modified form of the Iwan model that can capture both geometric and friction nonlinearity in a system. To do so, an element is added in parallel to the Jenkins elements, consisting of a nonlinear spring in series with a slider of infinite yield strength, i.e. $f^* = \infty$. The nonlinear spring corresponds to the SICE-ROM, defined to capture the geometrically nonlinear behavior. Since the slider associated with this nonlinear spring has infinite yield strength, it does not contribute to the hysteretic behavior exhibited by the Jenkins elements. The IGNL model is illustrated in Fig. 2.

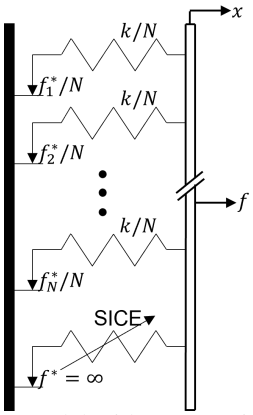

Figure 2: Illustration of the Iwan model with Geometric Nonlinearity, i.e. the IGNL model

The force-displacement relation for the added element is given by

$$f_{\text{gnl}} = \sum_{j=2}^{m} k_j x^j; \qquad \forall \dot{x}, \forall x \tag{13}$$

where m is the order of the SICE-ROM and k_j is the j^{th} nonlinear stiffness coefficient. Since this nonlinear element is in parallel to the rest of the Jenkins elements, its force contribution can be directly added to the total force-displacement relations described in Sec. 2.3. Thus, during initial loading, the force-displacement relation for the IGNL model, obtained by appending Eq. 11, is given by Eq. 14.

$$f = \sum_{i=1}^{n} \frac{f_i^*}{N} + \frac{k}{N} x(N-n) + \sum_{j=2}^{m} k_j x^j; \qquad \dot{x} > 0 \tag{14}$$

Similarly, the force-displacement relation when the displacement direction is reversed can be given by modifying Eq. 12, resulting in

$$f_{\text{rev}} = \sum_{i=1}^{n'} \frac{-f_i^*}{N} + \sum_{i=n'}^{n} \left[\frac{f_i^*}{N} - \frac{k}{N}(x^* - x) \right] + \frac{k}{N} x(N-n) + \sum_{j=2}^{m} k_j x^j; \qquad \dot{x} < 0,\ -x^* \leq x \leq x^*. \tag{15}$$

In Eqs. 13 – 15, it can be seen that the nonlinear force due to the added element does not show any hysteretic behavior; the same is true for all of the Jenkins elements that remain stuck. Therefore, the response of the added SICE element depends only on the current value of displacement and not its history. This property helps separate geometric nonlinearity from friction nonlinearity when fitting the proposed ROM to a specific FE model, as will be shown in the subsequent section.

3.2 Identifying the IGNL Model Using QSMA

As discussed in Sec. 2.1, the method of QSMA can be used to obtain the force-displacement relation for the nonlinear mode of interest. Given an FE model with both geometric and friction nonlinearity, the following procedure can be used to identify the IGNL model that can reproduce its nonlinear behavior, based on a few quasi-static simulations.

Consider the nonlinear mode r, the EoM for which can be written as

$$\ddot{q}_r + 2\zeta_{0,r}\omega_{0,r}\dot{q}_r + k_{\text{lin},r} q_r + \theta_{\text{nl}}(q_r, \boldsymbol{\theta}) = \boldsymbol{\Phi}_r^{\text{T}} \mathbf{f}_{\text{ext}}, \tag{16}$$

where $k_{\text{lin},r}$ is the linear stiffness excluding the stiffness due to the IGNL element, $\zeta_{0,r}$ is the linear damping, $\theta_{\text{nl}}(q_r, \boldsymbol{\theta})$ is the nonlinear restoring force in the modal domain that is a function of current displacement as well as previous states and is represented by Eqs. 14 and 15. The variables $q_r, \dot{q}_r, \ddot{q}_r$ are the nonlinear modal displacement, velocity and acceleration respectively. For the static case, the equation can therefore be reduced to

$$k_{\text{lin},r} q_r(\alpha) + \theta_{\text{nl}}(q_r, \boldsymbol{\theta}) = \boldsymbol{\Phi}_r^{\text{T}} \alpha \mathbf{M} \boldsymbol{\Phi}_r = \alpha. \tag{17}$$

The nonlinear restoring force, $\theta_{\mathrm{nl}}(q_r, \boldsymbol{\theta})$, comprises both geometric and frictional nonlinear effects. It can, therefore, be represented by the IGNL model. This means, during initial loading, the force-displacement relation (as per Eq. 14) is

$$\theta_{\mathrm{nl}} = \sum_{i=1}^{n} \frac{\hat{f}_i^*}{N} + \frac{\hat{k}}{N} q_r (N-n) + \sum_{j=2}^{m} \hat{k}_j q_r^j; \qquad \dot{q}_r > 0, \forall q_r. \tag{18}$$

Note, here, that $\hat{f}_i^*, \hat{k}$ and $\hat{k}_j$ are the equivalent of f_i^*, k and k_j in the modal domain, since $\theta_{\mathrm{nl}}(q_r, \boldsymbol{\theta})$ is a modal force. Now, in order to identify the coefficients of the SICE-ROM, $\hat{k}_j$, the force due to geometric nonlinearity needs to be isolated from the frictional effects. This can be achieved by setting the yield strength of all the Jenkins elements to infinity, i.e. $n = 0$ in Eq. 18. In an FE software, this is equivalent to setting the friction coefficient, $\mu = \infty$. The quasi-static problem in the modal domain then becomes

$$k_{\mathrm{lin},r} q_{r,\mathrm{stick}}(\alpha_{\mathrm{stick}}) + \theta_{\mathrm{nl,stick}}(\alpha_{\mathrm{stick}}) = \alpha_{\mathrm{stick}}, \tag{19}$$

where α_{stick} is the modal force amplitude, and $q_{r,\mathrm{stick}}(\alpha_{\mathrm{stick}})$ is the corresponding modal displacement calculated using QSMA. As discussed in Sec. 2.1, α takes discrete values over a range of force amplitudes to estimate the backbone curve. The nonlinear restoring force, $\theta_{\mathrm{nl,stick}}$ for this case can be written by substituting $n = 0$ in Eq. 18, resulting in

$$\theta_{\mathrm{nl,stick}} = \hat{k} q_{r,\mathrm{stick}} + \sum_{j=2}^{m} \hat{k}_j q_{r,\mathrm{stick}}^j; \qquad \dot{q}_{r,\mathrm{stick}} > 0, \forall q_{r,\mathrm{stick}}, \tag{20}$$

where $\hat{k}$ is equal to the sum of the stiffness values of all the linear springs in the IGNL model. Therefore, the total modal quasi-static force, α, according to Eq. 19, is a sum of the linear force, $(k_{\mathrm{lin},r} + \hat{k}) q_{r,\mathrm{stick}}$, and the nonlinear force due to the SICE-ROM. The linear stiffness, $(k_{\mathrm{lin},r} + \hat{k})$, must result in a frequency equal to the low-amplitude natural frequency of the r^{th} mode, $\omega_{0,r}$. Therefore,

$$k_{\mathrm{lin},r} + \hat{k} = \omega_{0,r}^2 \tag{21}$$

The coefficients of the polynomial constituting the SICE-ROM, k_j, can then be calculated from the force-displacement data, i.e. $\boldsymbol{\alpha}_{\mathrm{stick}}$ versus $\mathbf{q}_{r,\mathrm{stick}}$, by applying the method of least squares described in Sec. 2.2. Note, again, that $\boldsymbol{\alpha}_{\mathrm{stick}}$ and $\mathbf{q}_{r,\mathrm{stick}}$ are vectors since QSMA is performed over a range of force amplitudes.

Next, the slider strengths of the Jenkins elements that capture the hysteretic behavior due to friction need to be identified. A second quasi-static analysis is considered, this time with the yield strengths of the Jenkins elements being f_i^*/N. In an FE model, this corresponds to setting a finite friction coefficient, pre-determined based on the surface properties. Let $\boldsymbol{\alpha}_{\mathrm{slip}}$ be the vector of applied quasi-static force values and $\mathbf{q}_{r,\mathrm{slip}}$ be the corresponding displacement vector calculated using QSMA. This system obeys Eq. 17. Therefore,

$$k_{\mathrm{lin},r} \mathbf{q}_{r,\mathrm{slip}} + \boldsymbol{\theta}_{\mathrm{nl}} = \boldsymbol{\alpha}_{\mathrm{slip}}. \tag{22}$$

The vector $\boldsymbol{\theta}_{\mathrm{nl}}$ in the above equation is composed of both geometric and friction nonlinearity. Subtracting Eq. 19 from Eq. 22 in order to isolate the nonlinear force due to friction gives,

$$k_{\mathrm{lin},r} [\mathbf{q}_{r,\mathrm{slip}} - \mathbf{q}_{r,\mathrm{stick}}] + \boldsymbol{\theta}_{\mathrm{nl}} - \boldsymbol{\theta}_{\mathrm{nl,stick}} = \boldsymbol{\alpha}_{\mathrm{slip}} - \boldsymbol{\alpha}_{\mathrm{stick}}. \tag{23}$$

If a new vector of query points, $\mathbf{q}_r$, is defined over which both $\boldsymbol{\alpha}_{\mathrm{stick}}$ and $\boldsymbol{\alpha}_{\mathrm{slip}}$ are interpolated, Eq. 23 can be re-written as

$$\alpha_{\mathrm{slip}}(q_r) - \alpha_{\mathrm{stick}}(q_r) = \theta_{\mathrm{nl}}(q_r) - \theta_{\mathrm{nl,stick}}(q_r); \qquad \forall q_r. \tag{24}$$

Substituting Eqs. 18 and 20 in Eq. 24 gives

$$\alpha_{\mathrm{slip}}(q_r) - \alpha_{\mathrm{stick}}(q_r) = \sum_{i=1}^{n} \frac{\hat{f}_i^*}{N} + \frac{\hat{k}}{N} q_r (N-n) - \hat{k} q_r \qquad \dot{q}_r > 0, \forall q_r \tag{25}$$

$$= \theta_{\mathrm{hnl}}(q_r) \tag{26}$$

The first two terms on the right-hand side of Eq. 25 are similar to the total nonlinear force due to the Iwan model, given by Eq. 11. The linear term, $\hat{k} q_r$ gets subtracted since it was included as part of the SICE-ROM in Eq. 20. Therefore, what remains is the restoring force due to the underlying Iwan model that captures the effect of friction in the response of the nonlinear mode. Typically, the strengths of the sliders, $\hat{f}_i^*$ are defined by a parametric distribution function. However, this paper assumes the nonlinear force due to the Iwan model is quasi-linear in nature, i.e. the right-hand side of Eq. 25 can be linearized at each value of q_r and represented by a constant stiffness and dissipation at that amplitude. Section 3.3 further elaborates on how this dissipation and stiffness can be calculated using Masing's rules.

3.3 Estimating amplitude-dependent frequency and damping from the IGNL model

Nonlinear Normal Modes [36], or NNMs, are commonly used to represent the frequency-energy dependence in strongly nonlinear systems, such as structures with geometric nonlinearity. Peeters et al. [37] presented a shooting and pseudo-arclength numerical continuation method to compute NNMs. In simple terms, the shooting method estimates the periodic solution to a nonlinear equation of motion for a particular set of initial conditions using numerical time integration methods. Numerical continuation is simultaneously used to march along the NNM branch. Once the coefficients of the SICE-ROM have been estimated using the procedure described in Sec. 3.2, this shooting and continuation algorithm can be used to calculate the NNM of the SICE-ROM that constitutes the IGNL model. This NNM quantifies the change in the modal natural frequency, due to geometric nonlinearity, as a function of modal displacement amplitude, and has been represented in this paper as $\omega_{\mathrm{gnl}}(q_r)$. Since the element associated with the SICE-ROM in the IGNL model has infinite yield strength, it does not contribute to the damping of the overall system. Therefore, Eq. 20 can be written in quasi-linear form as

$$\theta_{\mathrm{nl,stick}} = \omega^2_{\mathrm{gnl}}(q_r)\, q_r. \tag{27}$$

On the other hand, Eq. 25 defines the hysteretic nonlinear force of the IGNL model. Since this nonlinearity is defined entirely by Jenkins elements, it behaves as a Masing Model [24, 25]. Therefore, Masing's rules can be applied to calculate the complete hysteretic loop at each modal amplitude level. The stiffness and damping can be estimated from these hysteresis loops, as described by Lacayo and Allen [27]. First, the change in stiffness at each displacement amplitude is given by the slope of the secant line at that amplitude, expressed mathematically by Eq. 28.

$$dK_{\mathrm{hnl}}(q_r) = \frac{\theta_{\mathrm{hnl}}(q_r)}{q_r}, \tag{28}$$

where $\theta_{\mathrm{hnl}}(q_r) = \alpha_{\mathrm{slip}}(q_r) - \alpha_{\mathrm{stick}}(q_r)$. The value of dK_{hnl} should be negative since the yielding of the Jenkins elements results in a loss of stiffness. Next, the area inside the loop equals the total energy dissipated at that amplitude level, represented as $D_{\mathrm{IGNL}}(q_r)$. This area can be evaluated numerically using the trapezoid rule at each amplitude. Figure 3 shows the hysteresis loop calculated for a representative displacement q using Masing's rules, and the corresponding secant stiffness and dissipation.

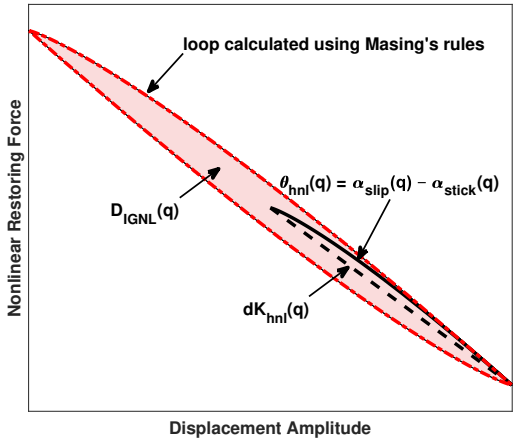

Figure 3: Illustrating the frequency and dissipation estimate due to hysteretic nonlinearity for amplitude q

Now, the amplitude-dependent behavior due to geometric nonlinearity (SICE-ROM) and hysteretic or friction nonlinearity (Masing model) need to be combined. From Eq. 28, $\theta_{\mathrm{hnl}}(q_r) = dK_{\mathrm{hnl}}(q_r)\, q_r$. Combining this with Eq. 27 gives

$$\theta_{\mathrm{nl,stick}} + \theta_{\mathrm{hnl}} = \omega^2_{\mathrm{gnl}}(q_r)\, q_r + dK_{\mathrm{hnl}}(q_r)\, q_r. \tag{29}$$

Therefore, the total stiffness can be calculated using Eq. 30,

$$K_{\mathrm{IGNL}}(q_r) = (\omega_{\mathrm{gnl}}(q_r))^2 + dK_{\mathrm{hnl}}(q_r). \tag{30}$$

The natural frequency, ω_{IGNL} is then given by

$$\omega_{\mathrm{IGNL}}(q_r) = \sqrt{K_{\mathrm{IGNL}}(q_r)}. \tag{31}$$

To estimate the effective damping at each amplitude level from the dissipation, the analogy of a viscous damper is used, as shown by Lacayo et al. [38]. At each amplitude, an equivalent viscous damper oscillating at frequency ω_{IGNL} while dissipation energy D_{IGNL} gives damping ratio ζ_{IGNL}, according to Eq. 32.

$$\zeta_{\mathrm{IGNL}}(q_r) = \frac{D_{\mathrm{IGNL}}(q_r)}{2\pi q_r^2(\omega_{\mathrm{IGNL}}(q_r))^2} + \zeta_{0,r} \tag{32}$$

In this way, the nonlinearity of the r^{th} mode can be characterized using the method of QSMA and the IGNL model.

Note that an alternative to applying Masing's rules would be to compute the complete hysteresis loop at each amplitude through QSMA itself. In this case, the force would need to be applied as an initial loading up to a positive amplitude followed by a reverse loading up to negative amplitude of the same magnitude and then a reloading back to the positive amplitude. However, Lengger and Wilner [39] show that the computational effort required to simulate the complete hysteresis loop at each amplitude makes this method significantly more expensive.

4 Numerical Case Study - SDOF System with Cubic Spring and Iwan Element

To test the validity of the above-presented method, a single degree-of-freedom (SDOF) system with a parallel arrangement of a cubic spring and Iwan element was considered, whose equation of motion is given below.

$$m\ddot{x} + 2\zeta_{\mathrm{lin}}\omega_0\dot{x} + K_\infty x + K_3 x^3 + \theta_{\mathrm{Iwan}}(x, \boldsymbol{\theta}) = f_{\mathrm{ext}}, \tag{33}$$

The four-parameter Iwan model [35], commonly used to represent bolted joint nonlinearity, was used to define the distribution of the slider strengths defining $\theta_{\mathrm{Iwan}}(x, \boldsymbol{\theta})$ in Eq. 33. The parameters of the system are listed in Table 1. The resulting system has a low-amplitude stuck frequency of 100 Hz, so $\omega_0 = \sqrt{K_\infty + K_{\mathrm{T}}} = 200\pi$. The cubic spring has a positive coefficient K_3, resulting in hardening behavior, i.e. the nonlinear stiffness due to this spring increases with increase in amplitude. The Iwan model, on the other hand, always exhibits softening behavior, i.e. it results in a decrease in stiffness with increasing amplitude. Thus, in this case study, the two nonlinearities can be understood to have opposing effects on the frequency.

Table 1: Properties of the nonlinear SDOF system used in the numerical case study

Parameter	Value
Mass (m)	1 kg
Linear macroslip stiffness (K_∞)	1.316×10^5 N/m
Material damping (ζ_{lin})	1×10^{-4}
Cubic spring stiffness (K_3)	5.396×10^{10} N/m^3
Iwan model $[F_{\mathrm{s}}, K_{\mathrm{T}}, \chi, \beta]$	[10000 N,2.632×10^5 N/m,-0.8,2]

As proposed in Sec. 3, two quasi-static analyses were performed. First, only the cubic spring was active, i.e. the Iwan element experienced no slip. This can be understood as replacing the nonlinear force due to the Iwan element in Eq. 33 with a linear spring of stiffness K_{T} representing the total stiffness of all of the sliders. Both of these are in parallel with the cubic spring. The low-amplitude linear frequency of the system equals the stuck frequency of 100 Hz. To estimate the force-displacement backbone curve, a linearly spaced force vector, $\mathbf{f}_{(\mathrm{nl},1)}$, from 1×10^{-4} N to 5000 N was defined. Note that a cubic spring results in symmetric force-displacement curves in the positive and negative loading directions. Therefore, only the positive loading curve is sufficient to fully identify the geometric nonlinearity exhibited. The displacement at each force value was then calculated by solving Eq. 34. Since this is a cubic equation, the roots could be calculated using Cardano's formula. However, the results presented here were obtained by solving the equation implicitly using the Newton-Raphson iteration scheme [40], so that the same numerical method could also be used when the Iwan model is considered in the subsequent quasi-static analysis. The resulting nonlinear displacement is represented here as $\mathbf{x_1}$. The dashed-dotted curve in Fig. 4a shows the force-displacement behavior obtained.

$$(K_\infty + K_{\mathrm{T}})\mathbf{x_1} + K_3\mathbf{x}_1^3 = \mathbf{f}_{(\mathrm{nl},1)} \tag{34}$$

In the second case, the complete system, including the four-parameter Iwan model, was considered. The nonlinear displacement, given by $\mathbf{x}_2$, was calculated by solving Eq. 35,

$$K_\infty \mathbf{x}_2 + K_3 \mathbf{x}_2^3 + f_j(\mathbf{x}_2, \phi) = \mathbf{f}_{(\mathrm{nl},2)} \tag{35}$$

where $f_\mathrm{j}(\mathbf{x}_2, \phi)$ is the nonlinear restoring force due to the four-parameter Iwan model for each value of $\mathbf{x}_2$, as given Eq. 36.

$$f_\mathrm{j}(\mathbf{x}_2, \phi) = \int_0^\infty \rho(\phi)[\mathbf{x}_2 - x_\mathrm{s}(\phi)]d\phi \tag{36}$$

Here, $x_\mathrm{s}(\phi)$ is the slider displacement, ϕ is the strength of the slider, and $\rho(\phi)$ is the density of sliders that have strength ϕ. Now, similar to case 1, Eq. 35 can be solved for $\mathbf{x}_2$ using the Newton-Raphson scheme. To do so, the integral in Eq. 36 needs to be discretized. This was done using the method outlined in [35], with a total of 100 discretization points or sliders. The resultant backbone curve for case 2 is given by the solid line in Fig. 4a.

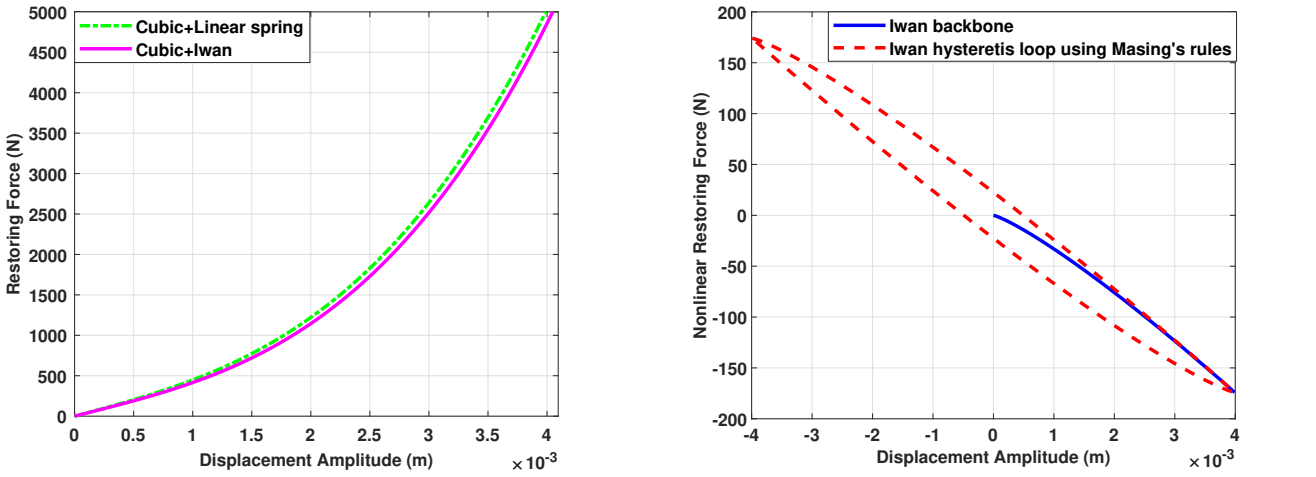

(a) (b)

Figure 4: (a) Force-displacement curve $\mathbf{f}_{(\mathrm{nl},1)}$ with all sliders stuck, i.e. when the cubic spring is in parallel with a linear spring (dashed-dotted curve), and curve $\mathbf{f}_{(\mathrm{nl},2)}$ when the cubic spring is in parallel with the Iwan element (solid curve), (b) The restoring force purely due to the Iwan element, obtained by subtracting the dashed-dotted curve from the solid curve in (a) (solid line) and the hysteresis loop at maximum amplitude, calculated using Masing's rules (dashed line)

As described in Sec. 3.2, the nonlinear restoring force purely due to the Iwan model can be obtained by subtracting the restoring force when only the cubic spring is active (i.e. case 1) from the restoring force obtained when both the cubic spring and the Iwan element are active (i.e. case 2). However, since the quasi-static analyses were performed by solving for the nonlinear displacement, the restoring force for case 2 was first interpolated linearly over the nonlinear displacement obtained for case 1, using Eq. 37,

$$f^*_{(\mathrm{nl},2)_i} = f_{(\mathrm{nl},2)_{i-}} + (x_{1_i} - x_{2_{i-}}) \left[\frac{f_{(\mathrm{nl},2)_{i+}} - f_{(\mathrm{nl},2)_{i-}}}{x_{2_{i+}} - x_{2_{i-}}} \right], \ \forall i \in [1, N] \tag{37}$$

where N is the length of the vector $\mathbf{x_1}$, $i+$ is the index of the first element of $f_{(\mathrm{nl},2)}$ that is greater than or equal to $f_{(\mathrm{nl},1_\mathrm{i})}$ and $i-$ is the index of the first element of $f_{(\mathrm{nl},2)}$ that is less than $f_{(\mathrm{nl},1_i)}$. The nonlinear restoring force purely due to the Iwan model, $\mathbf{f}_{\mathrm{nl,Iwan}}$ was then obtained using Eq. 38. Figure 4b shows this nonlinear force as a function of displacement.

$$\mathbf{f}_{\mathrm{nl,Iwan}} = \mathbf{f}^*_{(\mathrm{nl},2)} - \mathbf{f}_{(\mathrm{nl},1)} \tag{38}$$

Next, the amplitude-dependent frequency and damping were calculated from these backbone curves using the method outlined in Sec. 3.3. The effect of cubic spring alone on the frequency was estimated using the pseudo-arclength continuation method [37]. For the Iwan model, Masing's rules were applied to $\mathbf{f}_{\mathrm{nl,Iwan}}$ to estimate the complete hysteresis loop at every displacement amplitude. The dashed line in Fig. 4b shows the hysteresis loop calculated at the maximum amplitude. The area inside the hysteresis loop at each amplitude gave the dissipation due to the Iwan model at that amplitude, while Eq. 28 was used to calculate the loss of stiffness at that amplitude. Finally, the overall nonlinear frequency and damping was calculated using Eqs. 30-32.

The complete system's dynamic response to non-zero initial conditions was simulated to verify the quasi-static results. The displacement and state of the sliders at the end of the quasi-static analysis were used to define the initial conditions of the dynamic analysis. This means the initial displacement was set equal to the highest value of $\mathbf{x}_2$. A total of 100 sliders, or discretization points, were used, similar to the quasi-static analysis, and the initial positions of these sliders were set equal to the final positions calculated in the quasi-static analysis. The initial velocity and acceleration of the SDOF system was set to zero. The Newmark-β method [40] was used to integrate the nonlinear differential equations. Since this is an implicit integration technique, a Newton-Raphson iteration scheme must be used to converge to a solution at each time step. Shetty and Allen [41] provide the equations necessary to implement the Newmark-β method for an SDOF system with a single Iwan element. In the case presented here, the equations for the residue function, η_{NR}, and gradient, θ_{NR}, of the Newton-Raphson scheme need to be modified, with an additional term included to account for the cubic spring. Equations 39 and 40 describe the modified residue and gradient,

$$\eta_{\mathrm{NR}} = m\ddot{x}_{n+1} + C_{\mathrm{lin}}\dot{x}_{n+1} + K_\infty x_{n+1} + F_{\mathrm{nl}}(x_{n+1}, \boldsymbol{\phi}_{n+1}) + K_3 x_{n+1}^3 - F_{\mathrm{ext}}(t_{n+1}) \tag{39}$$

$$\theta_{\mathrm{NR}} = m + C_{\mathrm{lin}}\gamma_{\mathrm{nb}}\triangle t + [K_\infty + K_{\mathrm{nl}} + 3K_3 x_{n+1}^2]\beta_{\mathrm{nb}}(\triangle t)^2 \tag{40}$$

where $(n+1)$ represents the current time step, n represents the previous time step and $\triangle t$ is the step size. The nonlinear force due to the Iwan model, $F_{\mathrm{nl}}(x, \boldsymbol{\phi})$ and the corresponding stiffness $K_{\mathrm{nl}}(x, \boldsymbol{\phi})$ depend on the current displacement x and position of the sliders $\boldsymbol{\phi}$, a 100×1 vector, and are calculated for every iteration using the equations derived in [35]. The constants β_{NB} and γ_{NB} are pre-defined based on whether a constant or linear acceleration between time steps is assumed. Further details can be found in [41]. Figure 5 shows the evolution of displacement over time obtained after integration.

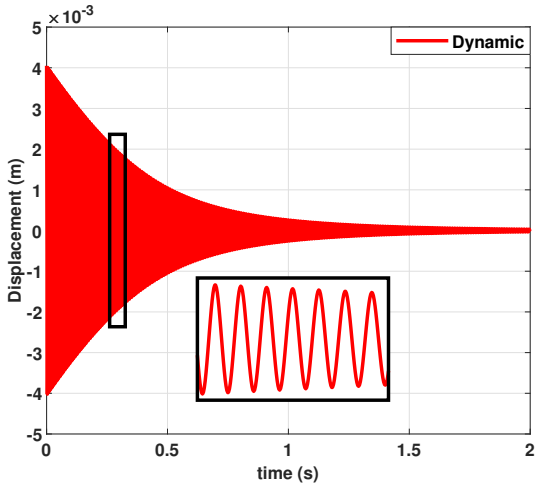

Figure 5: The true dynamic response (displacement vs time) for the SDOF model in Eq. 33, consisting of a cubic spring and an Iwan element

This dynamic response was then post-processed using the Hilbert transform [42] to estimate the amplitude-dependent frequency and damping. Figure 6a compares the amplitude-dependent frequency from the dynamic analysis (dashed line) against the IGNL model (solid line). The dashed-dotted line in Fig. 6a, $\omega_{\mathrm{n},3}(X)$, was obtained by using the pseudo-arclength continuation method to calculate the nonlinear normal mode (NNM) of the SDOF system with just a cubic spring. As can be seen, the Iwan element causes a noticeable change in frequency, especially at lower displacement amplitudes. Note here that both the dynamic analysis result (dashed line) and the final quasi-static result (solid line) eventually converge to the linear frequency value of 100 Hz at very low amplitudes, beyond the left edge of Fig 6a. There is good agreement between the true dynamic response and the IGNL model prediction at lower displacement amplitudes, with near zero error as seen in Fig. 6b. The error in frequency increases with amplitude, with a maximum error of 2.96%. While it is possible that the the proposed quasi-static method is less accurate as the level of nonlinearity increases at high amplitudes, it must be noted that the accuracy of the dynamic result itself is sensitive to the time-step used for the Newmark-β integration. As the frequency of oscillation of the system increases, the time-step must be decreased to mitigate integration error. For the results presented, a time-step $\triangle t = 1 \times 10^{-6}$s was used. Despite such a small step-size, it can be seen in Fig. 6a that the frequency estimated by the dynamic analysis at the highest amplitude is even higher than that due to just the cubic spring (dashed-dotted line). This is not realistic, though, since the cubic spring provides an upper bound to the expected hardening behavior.

Figure 7a plots the amplitude-dependent damping calculated from the dynamic analysis (dashed line) and the proposed method (solid line). Note that a traditional reduced order model, such as a SICE model, would not be able to predict the nonlinearity in the damping that is observed here, so one would have to assume a damping ratio based on material damping ($\zeta = 1 \times 10^{-4}$ in

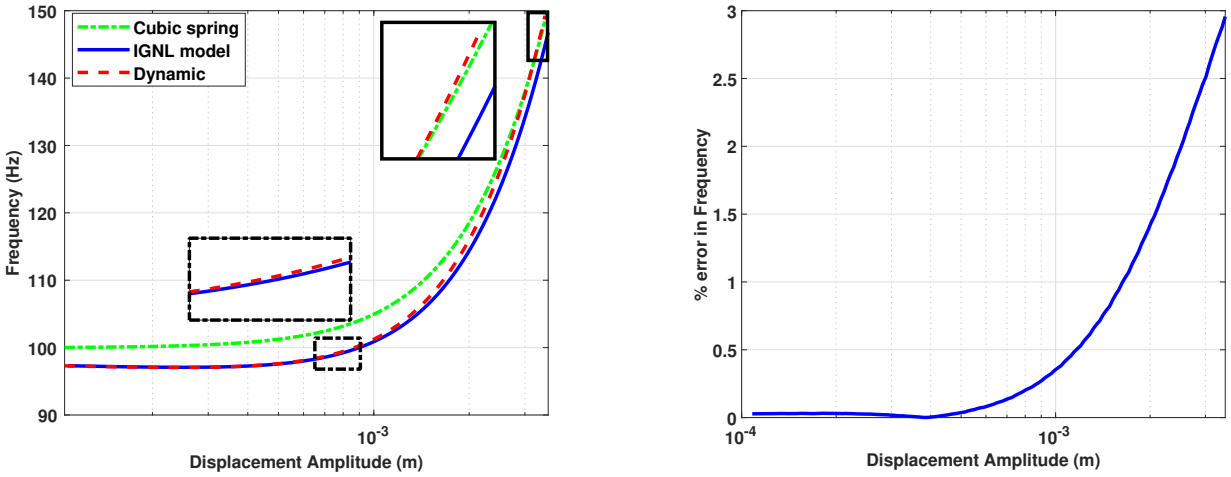

(a) (b)

Figure 6: (a) Comparison of the amplitude-dependent frequency estimated using the proposed method (solid curve) to the truth result (dashed curve) obtained by integrating Eq. 33. The dashed-dotted curve is the amplitude-dependent frequency change only due to the cubic spring, calculated using pseudo-arclength continuation. (b) The percentage error in frequency estimated using the proposed method, when compared to the truth result. Case where $K_3 = 5.396 \times 10^{10}$ N/m^3 (positive)

this case) or past experience. At low amplitudes, the proposed method gives an error of about 10%. This error decreases, and then increases, as the amplitude increases. The dotted line in this figure was obtained by calculating the damping as a function of the secant frequency estimated using Masing's rules instead of the final frequency estimate of the full IGNL model. As the amplitude increases, the dotted line significantly deviates from the dashed and solid lines. To explain this, consider Eq. 32, used to calculate the damping ratio from dissipation. The damping ratio at each amplitude is inversely proportional to the frequency at that amplitude. As the amplitude increases, the hardening effect of the cubic spring strongly influences the overall frequency, and this significant increase in frequency causes the damping ratio to decrease despite the dissipation increasing. This is why using the secant frequency gives inaccurate damping ratios at higher amplitudes, making it essential to account for the actual instantaneous frequency of the full IGNL model.

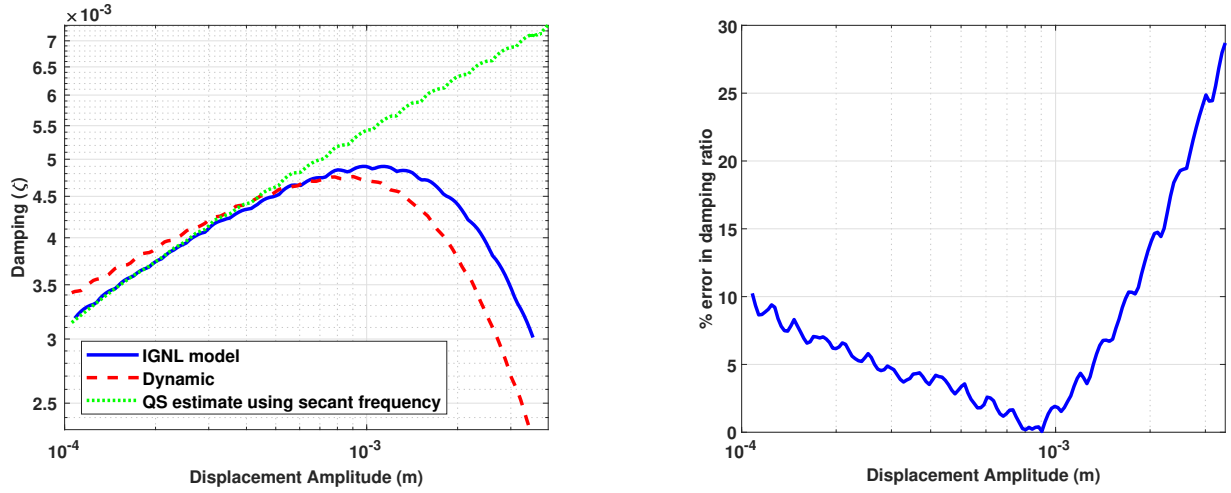

(a) (b)

Figure 7: (a) Comparison of the amplitude-dependent damping estimated using the proposed method (solid curve) to the truth result (dashed curve) obtained by integrating Eq. 33. The dotted curve represents the quasi-static estimate when using the secant frequency to calculate the damping ratio from the dissipation. (b) Percentage error in damping between the solid and dashed curves in (a). Case where $K_3 = 5.396 \times 10^{10}$ N/m^3 (positive).

Performing the dynamic analysis for this nonlinear SDOF system using the Newmark-β method with a time-step of $1 \times 10^{-6}s$ took $634.68s$ of processor time on an Intel(R) Core(TM) i7 CPU 950 @ 3.07GHz. On the other hand, the two quasi-static analyses and application of Masing's rules took $0.345s$, while the pseudo-arclength continuation algorithm to estimate the

frequency of the cubic spring took about $20s$, resulting in a total simulation time of $20.345s$. Thus, the proposed method is nearly 30 times faster than performing dynamic simulations to characterize the nonlinear behavior of the system.

A second case with negative cubic stiffness was considered, to evaluate the accuracy of the proposed method when both the cubic spring and the Iwan element exhibit softening behavior. A value of $K_3 = -5.395 \times 10^8$ N/m^3 was used, keeping all other parameters the same. The amplitude-dependent frequency and damping were estimated by following the exact same procedure as the one used for the positive cubic stiffness case. Figure 8a shows that the frequency estimated using the proposed method is in very good agreement with the dynamic results, with a maximum error of 0.41% at the highest amplitude. Figure 8b shows that the predicted amplitude-dependent damping is also in good agreement with the dynamic results. In fact, the proposed quasi-static method gives better results in this case than in the case of positive cubic stiffness. One reason for this could be that the proposed method is more effective when the Iwan, or friction, nonlinearity is the dominant form of nonlinearity. When the cubic spring stiffness is positive, the hardening effect dominates the overall system nonlinearity and opposes the Iwan element by reducing the number of sliders that can slip. On the other hand, the negative cubic stiffness results in softening behavior that assists, or amplifies the effect of, the Iwan element. Additionally, when the cubic spring stiffness is positive, the strong nonlinearity results in excitation of higher harmonics which may violate the quasi-linear assumptions used in the proposed method. On the other hand, the nonlinearity with negative cubic stiffness is less severe, obeying those assumptions.

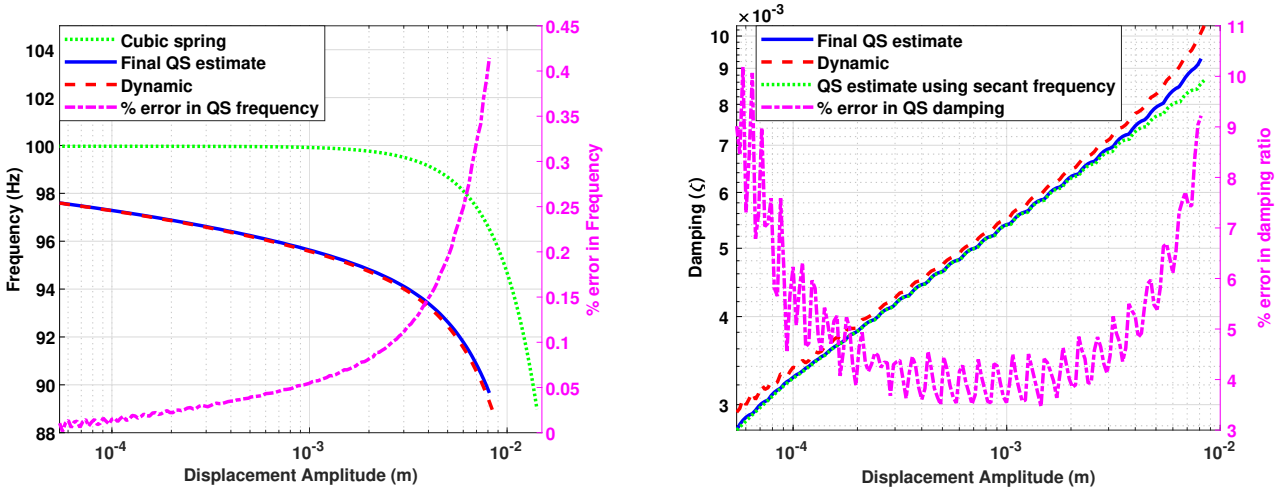

(a) (b)

Figure 8: (a) Amplitude dependent frequency (left axis) and percentage error in the frequency (right axis) when $K_3 = -5.395 \times 10^8$ N/m^3, and (b) the corresponding amplitude-dependent damping (left axis) and percentage error in damping (right axis)

5 Application to the Tribomechadynamics Benchmark Structure

Krack et al. [43] proposed a challenge - to perform a blind prediction of the dynamic behavior of a system with geometric and friction nonlinearity, referred to here as the Tribomechadynamics (or TMD) benchmark structure. A 3D CAD model of this structure is shown in Fig. 9. It consists of four main parts - a thin panel, a monolithic support comprising two pillars and a rear plate, and two blades. The panel is 1.5 mm thick, and is clamped between the blades and the support pillars using screws and washers. The surface of the support that is in contact with the panel has an inclination of about $1.1°$. Thus, the panel has some curvature when assembled. The bolted connections that clamp the panel to the support introduce friction nonlinearity in the structure, whereas the clamped panel itself exhibits geometric nonlinearity due to transverse deflection causing in-plane stresses (i.e bending-stretching coupling). The support is designed to be mounted to a shaker through a fixture along the rear plate. This benchmark structure was designed to be representative of real-world, industrial systems such as aircraft wing panels. The presence of both forms of nonlinearity makes this a challenging structure to study. Kuether et al. [33] found that it can take nearly 56 hours to simulate 0.25 s of dynamic response of a 3D FE model of the structure, using an HPC cluster with 9 nodes and 432 cores. This highlights the potential of a more computationally efficient approach, such as the one presented here.

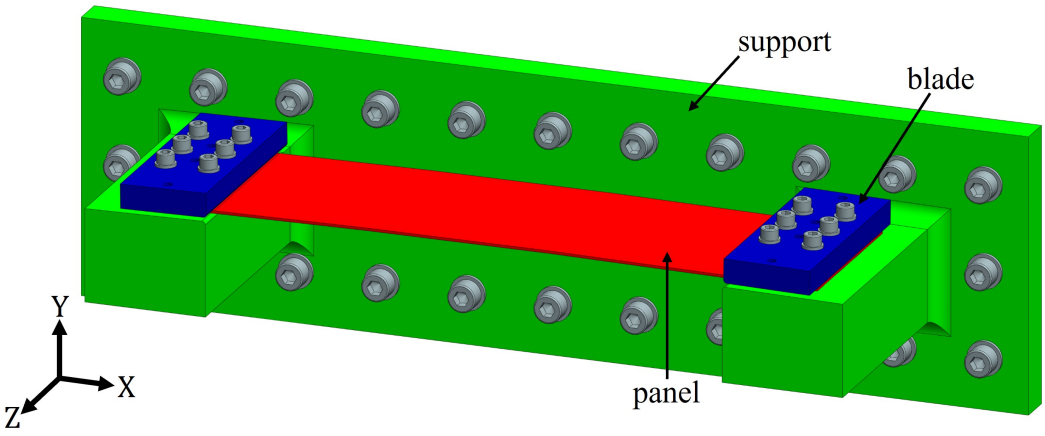

Figure 9: CAD model of the benchmark structure

The main aim of the challenge was to predict the nonlinear frequency and damping of the first bending mode of the system as a function of the displacement amplitude. To do so, first a suitable FE model needs to be created. Even quasi-static analyses of 3D FE models containing contact can be highly computationally expensive. For example, Wall et al. [44] found that a 3D model of two beams with held together using two lap joints required a minimum of 6 hours to perform a quasi-static analysis, with the solve-time climbing up to 48 hours if the contact surfaces were not initially flat. Therefore, a 2D FE model of the TMD structure was created to characterize its nonlinearity.

Certain approximations were made to model the 3D structure in 2D. First, the bolt preload was simulated by applying a pressure load along a line of length equal to the washer diameter. According to the model specifications, the fasteners clamping the panels at the ends are ISO 4762 - M6 screws, with a tensile strength of 800 MPa, and yield strength of $0.8 \times 800 = 640$ MPa. The applied preload is 90% of the yield strength. With a pitch diameter (d_p) of 5.35 mm and core diameter (d_c) of 4.773 mm for the M6 coarse series, the stress area can be calculated as $\pi(d_\mathrm{p}d_\mathrm{c})^2/16 = 20.1$ mm^2. Therefore, the applied preload equals 11578 N. The line pressure applied in the FE model was assumed to be an average of the total pressure acting along the depth of the support (or along the Z-axis), i.e. an average of the preload force acting on the area covered by the three washers and zero force acting on the rest of the area. Since the washers have a diameter of 12 mm, a pressure of 20.68 MPa was applied over a length of 12 mm. Note that the 2D FE model assumes unit thickness along the Z-axis.

Next, it was estimated that the stiffness arising due to the cantilever nature of the support-fixture arrangement is large enough for the support to behave as a rigid structure. Therefore, fixed translational and rotational boundary conditions were applied at all the nodes along the bottom edge of the support. This assumption was verified by creating a 3D model and comparing the linear frequencies for the two different boundary conditions [45].

Further, a Coulomb friction model, with a friction coefficient $\mu = 0.6$, was implemented to model the interface interactions. Three-node linear plane strain elements (i.e. CPE3 elements in Abaqus) were used to mesh all the parts. Initially, a mesh size of 1 mm was used near all the contact regions. After running a modal and quasi-static nonlinear analysis, this was refined further to better capture slip at the interfaces, reducing the size to $0.2 - 0.5$ mm. Five elements were used across the thickness of the panel. The mesh was gradually made coarser further away from the contact regions, with a maximum mesh size of 3 mm. The panel was modeled as flat and the application of line pressure in the preload step resulted in its curvature, as would be the case experimentally.

Figure 10 shows the 2D FE model that was created. The magnified version of the left-hand side contact interface shows the fine mesh that was used to capture the slip behavior at the interface. It also shows the panel modeled as flat with the support being at an angle, resulting in a gap between the two before the preload was applied. Note that the same mesh was replicated on the right-hand side interface.

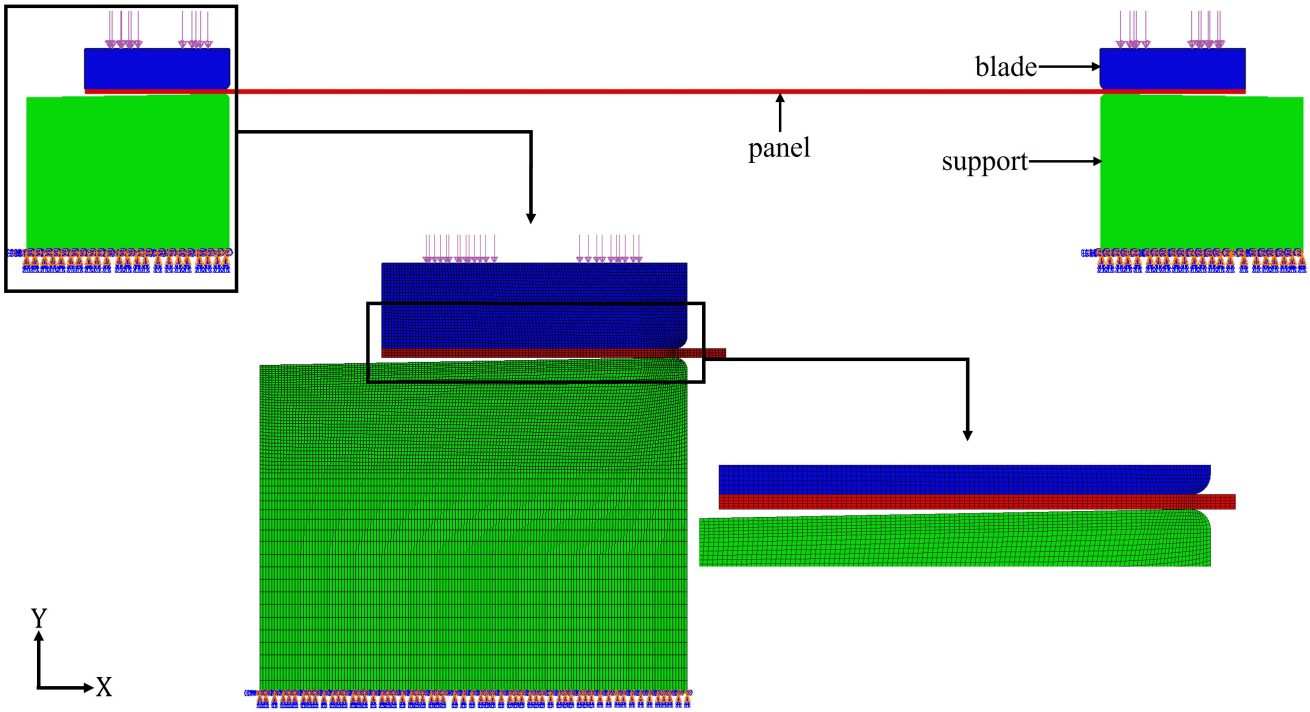

Figure 10: 2D FE model of the TMD structure, with a magnified version of the left-hand side interface showing the mesh density at contact

Figure 11 outlines the procedure used to estimate the amplitude-dependent frequency and damping for the TMD structure from the 2D FE model. The first step was a preload analysis, where the pressure applied resulted in 1) a negative bending moment on the panel and, 2) complete contact between the panel and the top surface of the support. This step estimated the contact pressure at the interfaces and the curvature of the panel when assembled. Step 1 was then followed by a linear modal analysis, step 2, estimating the linear frequencies and mode shapes of the first 15 modes. The linear frequency of mode 1 was found to be 118.12 Hz.

Step 3 was the main, quasi-static step, where concentrated loads were applied to load the FE model in the shape of mode 1. The mode shape calculated in step 2 was used to define the concentrated loads. Three separate quasi-static analyses - referred to, here, as A, B and C - were performed. For analysis A and B, the contact type at all interfaces was changed to not allow any slip between interfaces (i.e. $\mu = \infty$). In Abaqus, this corresponds to selecting the contact type as 'Rough' when defining the tangential behavior of the interaction property. In analysis A, the load was applied along the negative Y-axis, i.e. opposing the curvature of the panel while in analysis B the load was applied along the positive Y-axis. Both these analyses are required to fully characterize the geometric nonlinearity since the curvature of the panel results in unsymmetric behavior along the positive and negative loading directions. Analysis C had frictional contact with $\mu = 0.6$, same as the preload step. There is no difference in the loading of analyses B and C; the only difference is in the friction at the surfaces. A version of the modified Riks method [46] was used to solve the quasi-static step in all analyses. This method is suitable for highly nonlinear structures since it can capture any geometric instabilities when computing the force-displacement curve. In the modified Riks method, the scale of the loading is also solved for, using arclength continuation. Since the panel deflects by approximately 1.15 mm at the center by the end of the preload step, the maximum displacement at the center of the panel for stopping the quasi-static analysis was set to be 4.2 mm, resulting in a deflection approximately 3 mm (i.e. twice the thickness of the panel) in the quasi-static step.

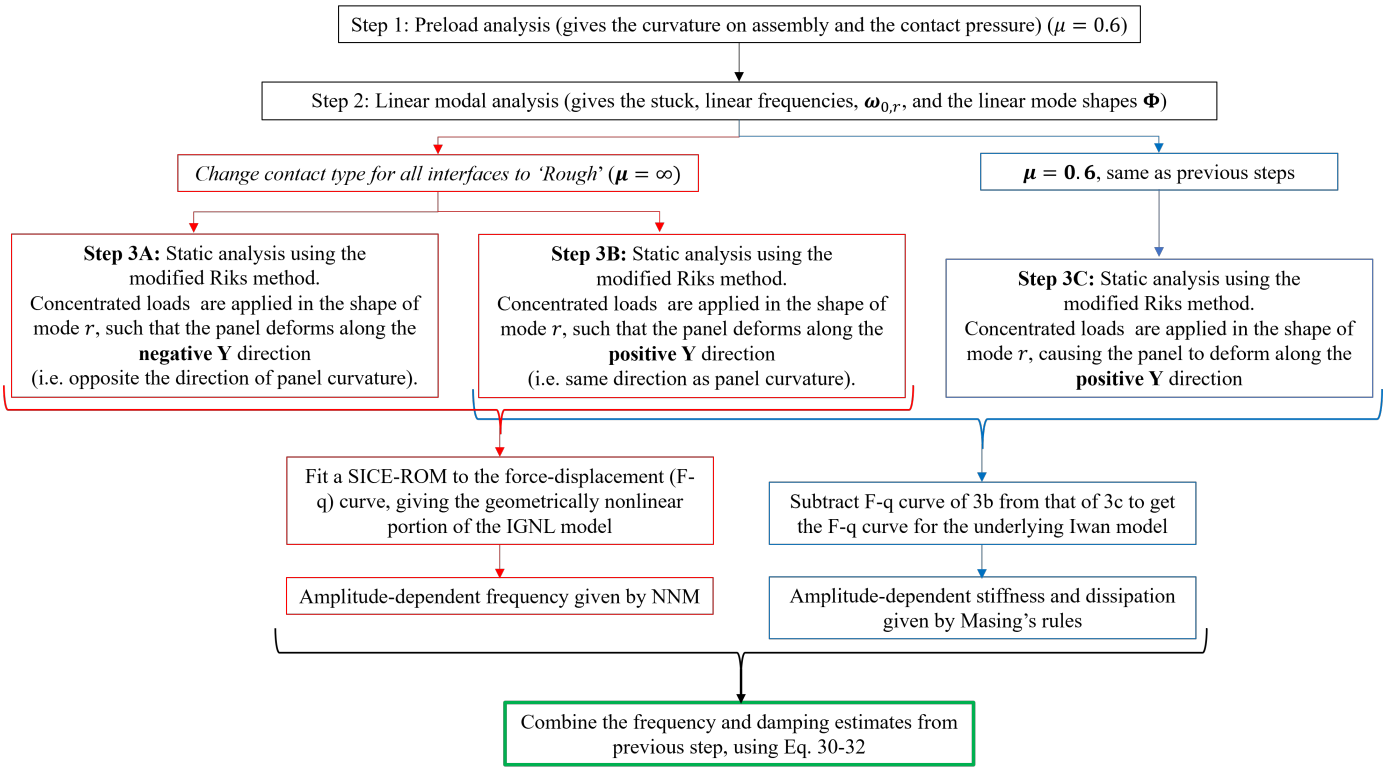

Figure 11: Flowchart summarizing the steps involved in estimating the amplitude-dependent nonlinearities from a full FE model using the proposed quasi-static approach and the IGNL model

Figure 12 shows the quasi-static force-displacement curves from analyses A and B. As anticipated, the curve is not symmetric in the positive and negative directions due to the curvature of the panel. The contribution of each mode to the displacement at the center of the panel was also plotted to check for static coupling between the modes. The displacement at the panel center due to mode r can be given as $x_{r,c} = \Phi_{r,c}^T q_r$, where c equals the node index corresponding to the panel center. Figure 13a shows the contribution of modes 1, 3, 5 and 7, the first four dominant modes. It can be seen that the third mode shows maximum static coupling to mode 1. The maximum displacement due to mode 3 was 0.306 mm, which is only 9.6% of the displacement due to mode 1. Therefore, the SICE-ROM was fit only to mode 1 and static coupling was neglected.

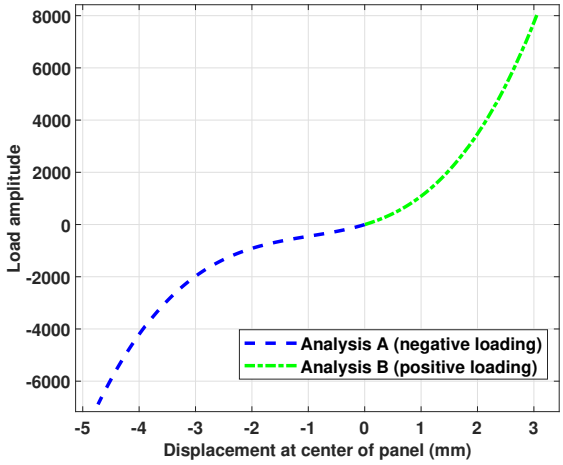

Figure 12: Quasi-static response when no slip allowed at interfaces. The load amplitude is plotted against the displacement of the center of the panel, as calculated using FEA.

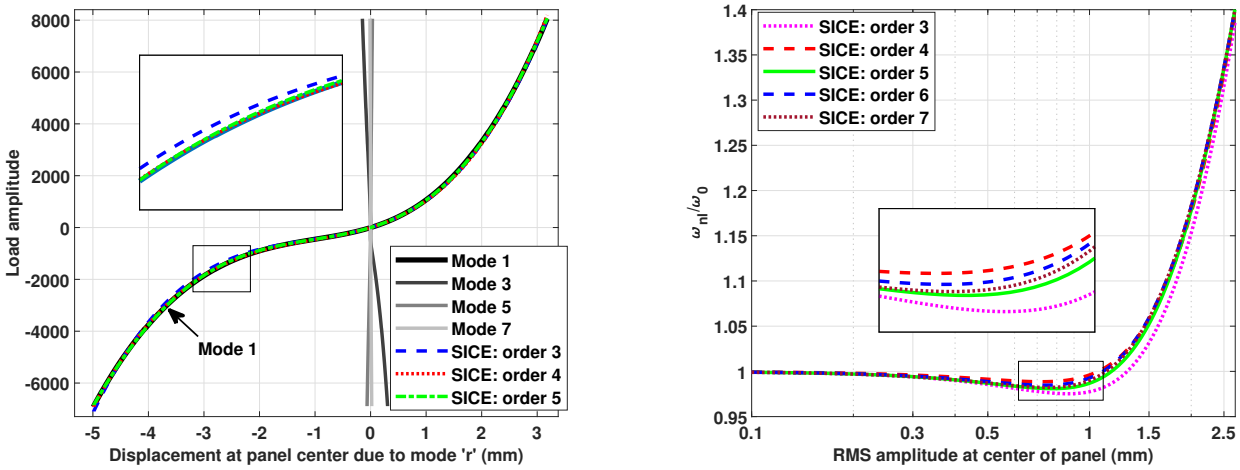

(a) (b)

Figure 13: (a) Quasi-static response of the four most dominant modes, when the load is applied in the shape of mode 1. The X-axis represents the contribution of each dominant mode to the displacement at the center of the panel, and the Y axis represents the load amplitude. The dashed, dotted and dashed-dotted lines show the 3rd, 4th and 5th order SICE polynomial fits respectively; (b) The frequency estimated by the SICE-ROMs of order 3-7 plotted against the root-mean-square (RMS) amplitude of the center of the panel. The frequency is non-dimensionalized by dividing by the linear frequency of mode 1, i.e. 118.12 Hz.

Third to seventh order SICE-ROMs were considered. As seen in Fig. 13a, the 3rd order ROM did not accurately fit the low-amplitude softening observed during negative loading. Additionally, higher order ROMs were able to capture the force-displacement behavior at high amplitudes better. Note that the 6th and 7th order fits have not been included in Fig. 13a for clarity. Figure 13b shows the amplitude-dependent frequency due to the SICE-ROMs of varying order, obtained by the arclength continuation method described in Sec. 3.3. The softening behavior between 0.5 mm and 1 mm corresponds to the low-amplitude softening observed in the negative loading direction in Fig. 13a. Additionally, it can be seen that the SICE-ROMs of odd order show more softening that those of even order. As the order of the ROM increases, the difference between the NNMs significantly decreases, with the NNMs from the 5th and 7th order ROMs nearly overlapping. Therefore, the 5th order SICE-ROM was used in the IGNL model.

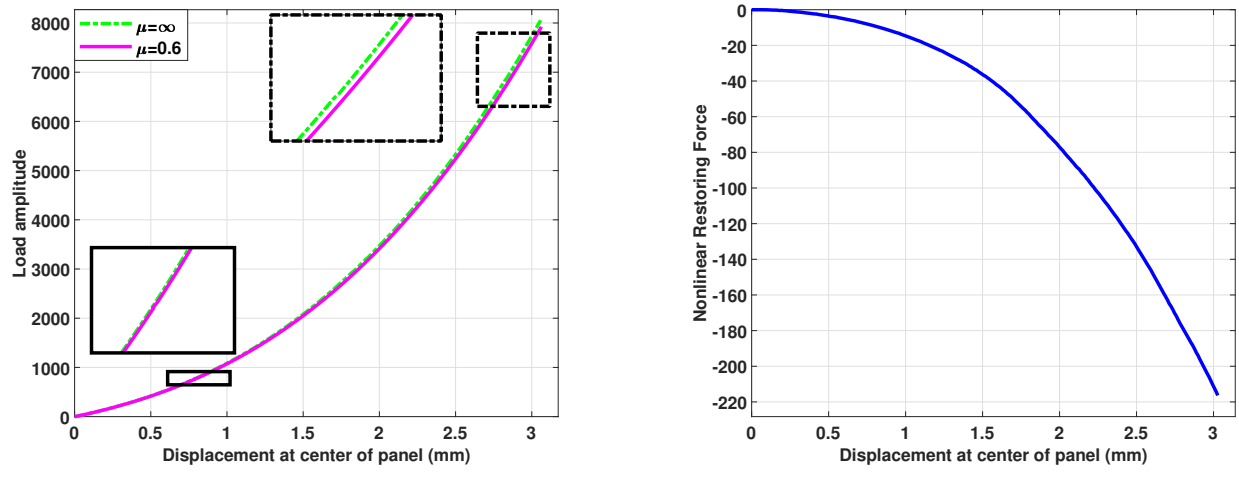

(a) (b)

Figure 14: (a) Force-displacement curve from analysis B (dashed-dotted curve), i.e. when the coefficient of friction is infinity, and from analysis C (solid curve), i.e. when the coefficient of friction is 0.6; (b) The restoring force purely due to friction, obtained by subtracting the dashed-dotted curve from the solid curve in (a)

On the other hand, analyses B and C were considered to characterize the friction nonlinearity of the mode, with their respective force-displacement curves shown in Fig. 14a. The force estimated from analysis B was subtracted from that of analysis C to

isolate the effect of friction. The resulting nonlinear restoring force due to friction is plotted against the displacement of the panel center in Fig. 14b. Masing's rules were then applied to estimate the change in stiffness and dissipation due to friction. Finally, the results of Masing's rules were combined with the NNM estimated by the 5th order SICE using the method described in Sec. 3.3. Figure 15a compares the amplitude-dependent frequency of the final IGNL model with the NNM of the 5th order SICE. At low displacement amplitudes, the frequency of the IGNL model is lower than the SICE-ROM, due to the decrease in stiffness as a result of friction. As the amplitude increases, the hardening behavior due to geometric nonlinearity dominates, leading to an overall increase in frequency. While the effect of friction on the frequency is small, its effect on the overall damping is significant, as seen in Fig. 15b. Note that the damping between 0.1 mm and 0.3 mm contains noise, likely due to the size of the mesh. An even finer mesh would be needed to capture slip at low amplitudes more accurately.

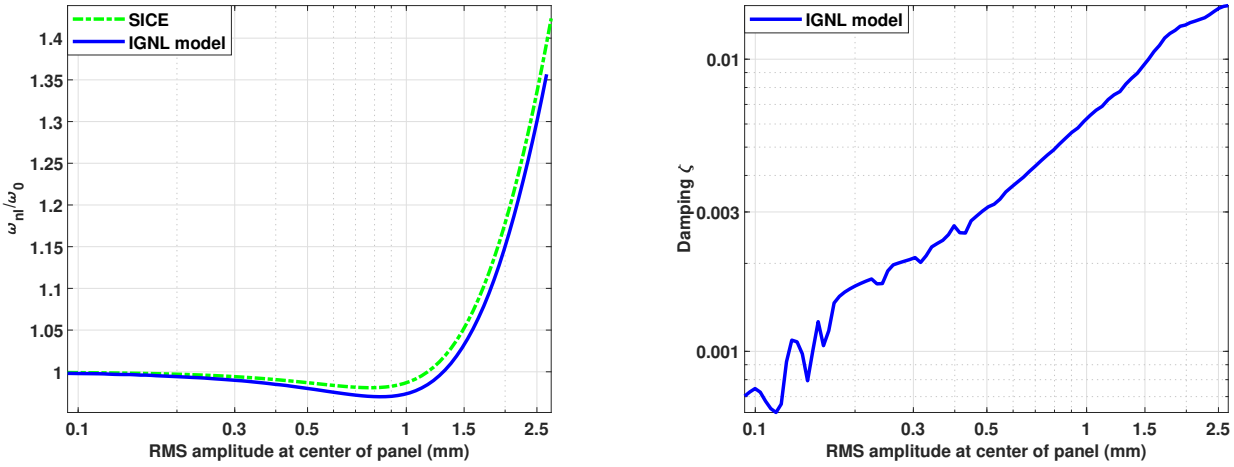

(a) (b)

Figure 15: (a) Non-dimensional frequency vs. RMS amplitude of the center of the panel, estimated from the 5th order SICE (dashed-dotted line) and from the full IGNL model (solid line); (b) Damping vs. RMS amplitude estimated by applying Masing's rules to the IGNL model

Table 2 shows the time taken to complete the above analysis on an Intel(R) i7-4790K CPU running at 4 GHz using 7 processors. The preload step required significant computational effort since the curvature of the panel was calculated in this step by the application of the preload force. The quasi-static analysis with infinite friction and negative loading, i.e. analysis A, required smaller increments at low amplitudes in comparison to analysis B, resulting in greater computational time. After completion of the quasi-static analysis, some post-processing is required to extract the force-displacement data from the output files. This process took longer than the quasi-static analysis itself, as shown in Table 2. Overall, the simulation took approximately 6 hours, which is significantly faster than performing a dynamic analysis [33]. Note that efforts are underway to implement some of these steps in Python or directly within the FEA package to further reduce the computational effort required.

Table 2: Time taken to estimate the frequency and damping of the TMD 2D FE model using QSMA and the IGNL model

Analysis	**Simulation time**
Preload Analysis	3912 s ($\approx$ 65 min.)
Linear Modal Analysis	3 s
QSMA - Analysis A	2069 s ($\approx$ 35 min.)
QSMA - Analysis B	1009 s ($\approx$ 17 min.)
QSMA - Analysis C	1413 s ($\approx$ 24 min.)
Post-processing QSMA output	$(3 \times 4080) = 12240$ s (≈ 3.4 h)
Frequency and damping computation	63 s
Total time taken	**5.75 h**

One of the assumptions made in the proposed method is that the system obeys Masing's rules. This was verified for the TMD model by applying Masing's rules to the force-displacement curve due to negative loading. For a hysteretic system that obeys Masing's rules, the above results should be valid even in the negative loading direction. For example, if the cubic spring in the

case study presented in Sec. 4 was replaced by a higher-order SICE-ROM that showed unsymmetric behavior in the positive and negative loading directions, the quasi-static identification approach used in Sec. 4 could be performed for either positive or negative loading, giving identical results. For the TMD model, this was tested by performing quasi-static analysis C with negative instead of positive loading. The nonlinear force from analysis A was then subtracted to check if the resulting nonlinear force-displacement curve is symmetric about the origin to the force-displacement curve from the positive loading case (plotted in Fig. 14b). Figure 16a shows the two quasi-static curves to be subtracted, and Fig. 16b compares the nonlinear force after subtraction against that obtained from positive loading. Note that, on subtraction, the restoring force due to friction in case of negative loading is in the second quadrant. However, in Fig. 16b, the curve has been mirrored about the origin by multiplying both the force and displacement vectors by -1 in order to easily compare it with the positive loading case. It can be seen that the curves from the positive and negative loading cases do not overlap. On studying the contact status, it was found that no slip occurs at the interfaces until the panel, which is concave at the start of the quasi-static step, deforms to a convex curvature. This explains why the frictional force is negligible up to a displacement value of 1.28 mm in Fig. 16b. Moreover, even after the onset of slip, the backbone curves obtained from positive and negative loading have different slopes, indicating different rates of slip. This implies that the hysteretic behavior of the FE model under consideration deviates from that due to a Masing model.

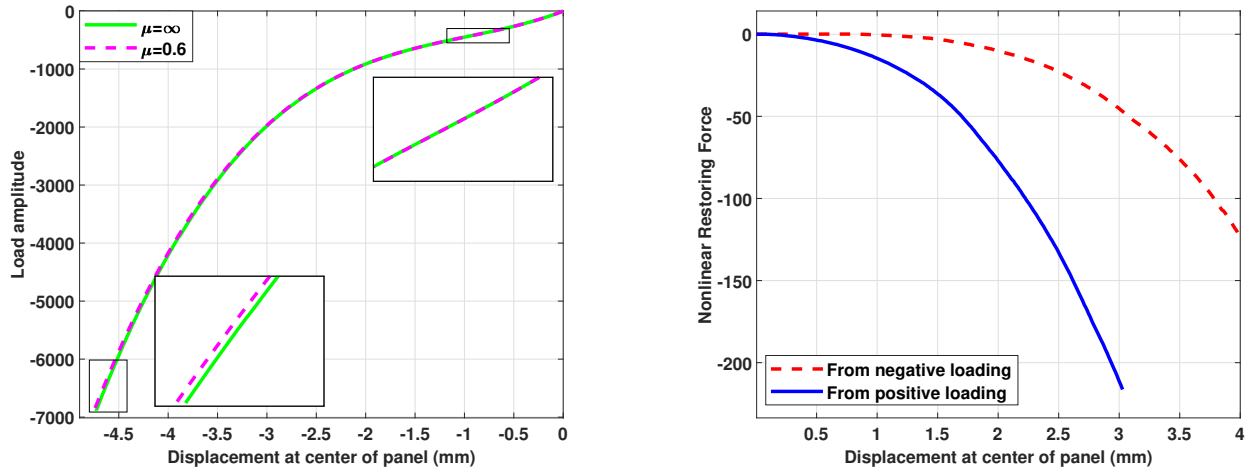

(a) (b)

Figure 16: (a) Force-displacement curve for negative loading when $\mu = \infty$ (dashed-dotted line), and when $\mu = 0.6$ (solid line); (b) Comparing the hysteretic nonlinear force from Eq. 23 obtained from the negative loading case (dashed line) and the positive loading case (solid line). Note that the dashed line is originally in the second quadrant, but the signs of the force and displacement vectors have been reversed to be able to visually compare it with the positive loading case.

Nevertheless, Masing's rules were applied to the force-displacement curve from the negative loading case to estimate the bounds of the amplitude-dependent frequency and damping using the IGNL model. As seen in Fig. 17a, in case of negative loading, friction has a negligible effect on the frequency. In an actual cycle of vibration the system would pass through both positive and negative displacements, and the natural frequency would represent an average of both. Therefore, one can expect that the positive loading case provides a lower bound for the frequency and the negative loading case can be understood as the upper bound. Figure 17b shows the damping estimated from the negative and positive loading cases. The damping in the negative loading case up to RMS amplitude of 0.5 mm is numerical, since no slip occurs at the interfaces up to this point. Beyond 0.5 mm, the damping increases, but is less than the damping obtained from the positive loading case. Considering that the actual damping is due to the energy dissipated as the system moves through both positive and negative displacements, the true damping can be expected to lie between the two values estimated using the positive and negative loading curves.

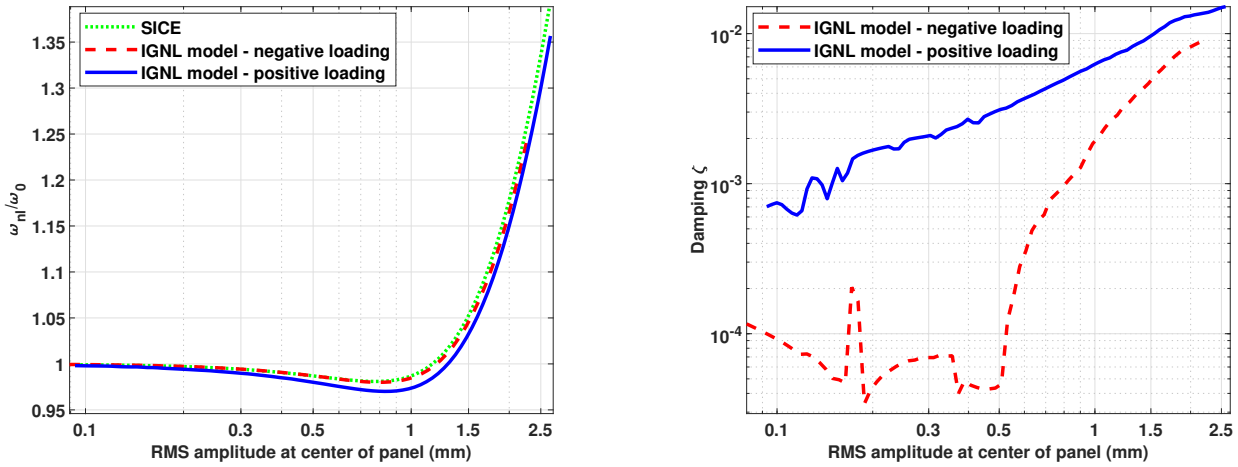

(a) (b)

Figure 17: Comparison of the (a) non-dimensional frequency vs. RMS amplitude of the center of the panel, and (b) Damping vs. RMS amplitude, estimated using the IGNL model that was identified by applying a positive quasi-static load (solid lines) and a negative quasi-static load (dashed lines)

6 Conclusions

This paper presented a novel reduced-order modeling approach to predict the amplitude-dependent frequency and damping of a system comprising geometric and friction nonlinearity. A numerical case study of an SDOF system with a cubic spring and Iwan element in parallel was considered to test the accuracy and speed of the proposed approach. A maximum error of 2.96% in frequency and 25% in damping was observed, with the error being highest at larger amplitudes. The proposed method was found to be nearly 30 times faster than simulating the dynamic response of the system. A 2D FE model of a structure with a thin panel clamped at the ends using mechanical fasteners was considered. The paper showed how the interaction properties of the FE model can be varied to isolate the geometric and friction nonlinearities. For this 2D model, preload analysis took about 1 hour and the three quasi-static analyses that were used took about 0.5 hours each. This represents the minimum computations that could be performed to fit an IGNL model to the measurements, assuming Masing's rules are applicable. Moreover, the IGNL model can be used to speed up further simulations of the system rather than integrating high-fidelity models. However, it was observed that the hysteretic behavior of the TMD model deviated from that due to a Masing model, adding significant uncertainty to the frequency and damping predictions. Alternatively, quasi-static simulations could have been performed for a complete cycle by applying loading, unloading and reloading forces. This would have to be repeated at each amplitude of interest to characterize the behavior without using Masing's rules. The simulation of each hysteresis loop would approximately take an additional $0.5 \times 2 = 1$ hour. Therefore, if the hysteresis loops at N force amplitudes are required, the additional computation time would be N hours. While this could improve the accuracy of the IGNL model, it must be noted that the model is inherently Masing in nature and wouldn't be able to capture non-Masing behavior accurately. Regardless, the proposed approach provides a range for the nonlinear frequency as well as damping by taking into account both geometric and friction nonlinearity, something that cannot be done by existing reduced-order models. In the future, other, non-Masing hysteretic models can be considered instead of the Iwan model, to further improve the accuracy and flexibility of the proposed approach.

References

[1] S. Woinowsky-Krieger. The Effect of an Axial Force on the Vibration of Hinged Bars. *Journal of Applied Mechanics*, 17(1):35–36, April 2021.

[2] I. S. Raju, G. Venkateswara Rao, and K. Kanaka Raju. Effect of longitudinal or inplane deformation and inertia on the large amplitude flexural vibrations of slender beams and thin plates. *Journal of Sound and Vibration*, 49(3):415–422, December 1976.

[3] E. J. Richards and D. J. Mead. *Noise and Acoustic Fatigue in Aeronautics*. Chichester, United Kingdom: John Wiley & Sons Ltd, London New York Sydney Toronto, 1st edition edition, 1968.

[4] E.E. Ungar. The Status of Engineering Knowledge Concerning the Damping of Built-up Structures. *Journal of Sound and Vibration*, 26(1):141–154, 1973.

[5] L. Gaul and J. Lenz. Nonlinear Dynamics of Structures Assembled by Bolted Joints. *Acta Mechanica*, 125(1):169–181, 1997.

[6] David O. Smallwood, Danny Lynn Gregory, and Ronald G. Coleman. Damping Investigations of a Simplified Frictional Shear Joint. Technical Report SAND2000-1929C, Sandia National Lab. (SNL-NM), Albuquerque, NM (US);Sandia National Labs., Livermore, CA (US), 2000.

[7] Brandon J. Deaner, Matthew S. Allen, Michael J. Starr, Daniel J. Segalman, and Hartono Sumali. Application of Viscous and Iwan Modal Damping Models to Experimental Measurements From Bolted Structures. *Journal of Vibration and Acoustics*, 137(2):021012, 2015.

[8] Daniel R. Roettgen and Matthew S. Allen. Nonlinear Characterization of a Bolted, Industrial Structure Using a Modal Framework. *Mechanical Systems and Signal Processing*, 84:152 – 170, 2017.

[9] J. Lenz and L. Gaul. The Influence of Microslip on the Dynamic Behavior of Bolted Joints. In *Proceedings of the International Modal Analysis Conference (IMAC XXIII)*, pages 248–254, Nashville, TN, 1995.

[10] Eric E. Ungar. Energy Dissipation at Structural Joints; Mechanisms and Magnitudes:. Technical report, Defense Technical Information Center, Fort Belvoir, VA, 1964.

[11] D. J. Segalman and C. R. Dohrmann. A Method for Calculating the Dynamics of Rotating Flexible Structures, Part 1: Derivation. *Journal of Vibration and Acoustics*, 118(3):313–317, July 1996.

[12] Marc P. Mignolet, Adam Przekop, Stephen A. Rizzi, and S. Michael Spottswood. A review of indirect/non-intrusive reduced order modeling of nonlinear geometric structures. *Journal of Sound and Vibration*, 332(10):2437–2460, May 2013.

[13] Robert J. Kuether, Brandon J. Deaner, Joseph J. Hollkamp, and Matthew S. Allen. Evaluation of Geometrically Nonlinear Reduced-Order Models with Nonlinear Normal Modes. *AIAA Journal*, 53(11):3273–3285, November 2015.

[14] Alexander A Muravyov and Stephen A Rizzi. Determination of nonlinear stiffness with application to random vibration of geometrically nonlinear structures. *Computers & Structures*, 81(15):1513–1523, July 2003.

[15] M. I. Mcewan, J. R. Wright, J. E. Cooper, and A. Y. T. Leung. A Combined Modal/Finite Element Analysis Technique for the Dynamic Response of a Non-Linear Beam to Harmonic Excitation. *Journal of Sound and Vibration*, 243(4):601–624, June 2001.

[16] Joseph J. Hollkamp and Robert W. Gordon. Reduced-Order Models for Nonlinear Response Prediction: Implicit Condensation and Expansion. *Journal of Sound and Vibration*, 318(4):1139–1153, December 2008.

[17] Kyusic Park and Matthew S. Allen. Quasi-Static Modal Analysis for Reduced Order Modeling of Geometrically Nonlinear Structures. *Journal of Sound and Vibration*, 502:116076, June 2021.

[18] D. J. Segalman. Modelling Joint Friction in Structural Dynamics. *Structural Control and Health Monitoring*, 13(1):430–453, 2006.

[19] L. Gaul and R. Nitsche. The Role of Friction in Mechanical Joints. *Applied Mechanics Reviews*, 54(2):93–106, March 2001.

[20] Allen T. Mathis, Nidish N. Balaji, Robert J. Kuether, Adam R. Brink, Matthew R. W. Brake, and D. Dane Quinn. A Review of Damping Models for Structures With Mechanical Joints1. *Applied Mechanics Reviews*, 72(4):040802, July 2020.

[21] P. R. Dahl. A Solid Friction Model:. Technical report, Defense Technical Information Center, Fort Belvoir, VA, May 1968.

[22] K. C. Valanis. A Theory of Visco-Plasticity Without a Yield Surface, Part I: General Theory. *Archives of Mechanics*, 23:535, 1971. Publisher: ARCHIVES OF MECHANICS.

[23] W. D. Iwan. A Distributed-Element Model for Hysteresis and Its Steady-State Dynamic Response. *Journal of Applied Mechanics*, 33(4):893–900, December 1966.

[24] G Masing. Self-stretching and hardening for brass. In *Proceedings of the 2nd International Congress for Applied Mechanics*, pages 332–335, Zurich, Switzerland, 1926.

[25] Paramsothy Jayakumar. *Modeling and identification in structural dynamics*. Report or Paper, California Institute of Technology, Pasadena, CA, May 1987. Issue: 87-01 Number: 87-01 Publisher: California Institute of Technology.

[26] Daniel Joseph Segalman. A Modal Approach to Modeling Spatially Distributed Vibration Energy Dissipation. Technical Report SAND2010-4763, 993326, Sandia National Lab., Albuquerque, NM, 2010.

[27] Robert M. Lacayo and Matthew S. Allen. Updating structural models containing nonlinear Iwan joints using quasi-static modal analysis. *Mechanical Systems and Signal Processing*, 118:133–157, March 2019.

[28] Hugo Festjens, Gaël Chevallier, and Jean-luc Dion. A Numerical Tool for the Design of Assembled Structures Under Dynamic Loads. *International Journal of Mechanical Sciences*, 75:170–177, October 2013.

[29] Emily Jewell, Matthew S. Allen, Iman Zare, and Mitchell Wall. Application of quasi-static modal analysis to a finite element model and experimental correlation. *Journal of Sound and Vibration*, 479:115376, August 2020.

[30] Mitchell Wall, Iman Zare, and Matthew S Allen. Predicting S4 Beam Joint Nonlinearity Using Quasi-Static Modal Analysis. In *38th International Modal Analysis Conference (IMAC XXXVIII)*. Springer International Publishing, February 2020.

[31] Iman Zare and Matthew S. Allen. Adapting a Contact-Mechanics Algorithm to Predict Damping in Bolted Joints Using Quasi-Static Modal Analysis. *International Journal of Mechanical Sciences*, 189:105982, January 2021.

[32] Nidish Narayanaa Balaji and Matthew R. W. Brake. A quasi-static non-linear modal analysis procedure extending Rayleigh quotient stationarity for non-conservative dynamical systems. *Computers & Structures*, 230:106184, April 2020.

[33] Robert J. Kuether, David A. Najera, Jonel Ortiz, Moheimin Y. Khan, and Paul R. Miles. 2021 Tribomechadynamics Research Challenge: Sandia National Laboratories High-Fidelity FEA Approach, February 2022. presented at 40th International Modal Analysis Conference (IMAC-XL).

[34] Malte Krack, Christoph Schwingshackl, and Matthew R Brake. The Tribomechadynamics Research Challenge. In *40th International Modal Analysis Conference (IMAC-XL)*, page 3. Springer International Publishing, February 2022.

[35] Daniel J. Segalman. A Four-Parameter Iwan Model for Lap-Type Joints. *Journal of Applied Mechanics*, 72(5), 2005.

[36] G. Kerschen, M. Peeters, J. C. Golinval, and A. F. Vakakis. Nonlinear Normal Modes, Part I: A Useful Framework for the Structural Dynamicist. *Mechanical Systems and Signal Processing*, 23(1):170–194, January 2009.

[37] M. Peeters, R. Viguié, G. Sérandour, G. Kerschen, and J. C. Golinval. Nonlinear Normal Modes, Part II: Toward a Practical Computation Using Numerical Continuation Techniques. *Mechanical Systems and Signal Processing*, 23(1):195–216, January 2009.

[38] Robert M. Lacayo, Brandon J. Deaner, and Matthew S. Allen. A Numerical Study on the Limitations of Modal Iwan Models for Impulsive Excitations. *Journal of Sound and Vibration*, 390:118–140, 2017.

[39] Michael Lengger and Kai Willner. Application of Quasi-Static Modal Analysis to the Tribomechadynamics Benchmark System, July 2021. presented at Tribomechadynamcis Research Conference.

[40] Robert D. Cook, David S. Malkus, Michael E. Plesha, and Robert J. Witt. *Concepts and Applications of Finite Element Analysis*. John Wiley & Sons, New York, 2007.

[41] Drithi Shetty and Matthew Allen. Fast Simulation of a Single Degree-of-Freedom System Consisting of An Iwan Element Using the Method of Averaging. *Journal of Vibration and Acoustics*, 142(5):051107, October 2020.

[42] Michael Feldman. Non-Linear System Vibration Analysis Using Hilbert Transform–I. Free Vibration Analysis Method 'Freevib'. *Mechanical Systems and Signal Processing*, 8(2):119–127, March 1994.

[43] Malte Krack and Johann Gross. *Harmonic Balance for Nonlinear Vibration Problems*. Mathematical Engineering. Springer International Publishing, Cham, 2019.

[44] Mitchell Wall, Matthew S. Allen, and Robert J. Kuether. Observations of modal coupling due to bolted joints in an experimental benchmark structure. *Mechanical Systems and Signal Processing*, 162:107968, January 2022.

[45] Drithi Shetty, Kyusic Park, Courtney Payne, and Matthew S. Allen. Predicting Nonlinearity in the TMD Benchmark Structure Using QSMA and SICE. In *Nonlinear Structures & Systems, Volume 1*, pages 281–287, Cham, February 2022. Springer International Publishing. Series Title: Conference Proceedings of the Society for Experimental Mechanics Series.

[46] E. Riks. An incremental approach to the solution of snapping and buckling problems. *International Journal of Solids and Structures*, 15(7):529–551, January 1979.